

Printed enzymatic glucose/air batteries: performance, stability and mass-manufacturing

Saara Tuurala



Printed enzymatic glucose/air batteries: performance, stability and mass- manufacturing

Saara Tuurala

A doctoral dissertation completed for the degree of Doctor of Science (Technology) to be defended, with the permission of the Aalto University School of Chemical Engineering, at a public examination held at the lecture hall Ke2 of the school on 19 May 2017 at 12.

Aalto University
School of Chemical Engineering
Department of Chemistry and Materials Science

Supervising professor

Associate Professor Lasse Murtomäki, Aalto University, Finland

Thesis advisors

Associate Professor Tanja Kallio, Aalto University, Finland

Research Team Leader Dr Maria Smolander, Technical Research Centre of Finland Ltd, Finland

Preliminary examiners

Associate Professor Scott Calabrese Barton, Michigan State University, The United States of America

Reader Daren Caruana, University College London, England

Opponent

Professor Edmond Magner, University of Limerick, Ireland

Aalto University publication series

DOCTORAL DISSERTATIONS 83/2017

VTT SCIENCE 152

© 2017 Saara Tuurala

ISBN 978-952-60-7412-2 (printed)

ISBN 978-952-60-7411-5 (pdf)

ISSN-L 1799-4934

ISSN 1799-4934 (printed)

ISSN 1799-4942 (pdf)

<http://urn.fi/URN:ISBN:978-952-60-7411-5>

ISBN 978-951-38-8537-3 (printed)

ISBN 978-951-38-8536-6 (pdf)

ISSN-L 2242-119X

ISSN 2242-119X (printed)

ISSN 2242-1203 (pdf)

<http://urn.fi/URN:ISBN:978-951-38-8536-6>

Unigrafia Oy

Helsinki 2017

Finland



Author

Saara Tuurala

Name of the doctoral dissertation

Printed enzymatic glucose/air batteries: performance, stability and mass-manufacturing

Publisher School of Chemical Engineering

Unit Department of Chemistry and Materials Science

Series Aalto University publication series DOCTORAL DISSERTATIONS 83/2017

Field of research Chemistry

Manuscript submitted 13 January 2017

Date of the defence 19 May 2017

Permission to publish granted (date) 20 March 2017

Language English

Monograph

Article dissertation

Essay dissertation

Abstract

The enzymatic biofuel cell (EBFC) converts the chemical energy of biofuel into electricity via bioelectrochemical reactions. The use of enzymes confers many advantages over metal catalysts e.g. renewability and low toxicity. However, enzymes are fairly sensitive to changes in temperature, pH and moisture. For this reason, enzymes are typically immobilized on electrodes either by chemical or physical adsorption. The electrodes are usually immersed in a liquid cell containing an optimised electrolyte. Hence, the conventional EBFC configuration is not practical and for this reason, a new type of EBFC was developed.

In this thesis, screen printed enzymatic electrodes (4-12 cm²) were fabricated on paper-based substrates using enzymatic inks creating thin (ca. 1 mm) and bendable EBFCs. The outcome of this thesis was a mass-manufacturable glucose/air biobattery that can be stored as dry and activated on demand by buffer. The power output of these biobatteries was on μW scale, however multiple suggestions for achieving higher performance are presented in this thesis. This biobattery could be integrated e.g. with low-power sensors, RFID tags or even cosmetic/medical skin patches.

At the anode, commercial glucose oxidase (GOx) and in-house purified aldose dehydrogenase (ALDH) were studied. At the cathode, two in-house purified laccases from *Trametes hirsuta* (ThL) and recombinant *Melanocarpus albomyces* were studied as well as one industrial laccase (EcoL). The fabrication methods included ink formulation using different carbon supports, biocompatible binders and enzyme-mediator pairs. First printing trials were performed in the laboratory using multiple enzyme-mediator pairs mixed with a commercial carbon-based ink. After that, the manufacturing was scaled up using GOx and EcoL mixed with in-house prepared graphite-based inks. The printed EBFCs were mainly characterised by means of electrochemistry.

In the laboratory, the best power output ($P_{\max} = 3.5 \mu\text{W cm}^{-2}$) was achieved with an ALDH/ThL cell, which had an open circuit voltage (OCV) of 0.62 V and maximum energy output (E) of ca. 10 μWh cm⁻². The best GOx/ThL cell had an OCV of 0.38 V, P_{\max} of 1.4 μW cm⁻² and E of 5.5 μWh cm⁻². The pilot scale manufactured GOx/EcoL cells performed 50-90% less, which could be attributed to differences in the ink compositions as well as to the degradation of enzyme-mediator electrodes due to heating (23 °C vs. 70 °C) and storage (one day vs. one week). The stability of the printed enzymes (GOx and EcoL) was very good, they lost a maximum of 40% of their activity, regardless of the drying or storage temperature. However, when mediators were added into the inks, elevated drying temperatures accelerated the degradation, and 70-80% of the enzymatic activity was lost in 28 days. Moreover, the anode was found to be the limiting factor, and for this reason different approaches to increase the anode performance were tested.

Keywords enzymatic biofuel cell, enzymatic electrodes, biobattery, screen printing

ISBN (printed) 978-952-60-7412-2

ISBN (pdf) 978-952-60-7411-5

ISSN-L 1799-4934

ISSN (printed) 1799-4934

ISSN (pdf) 1799-4942

Location of publisher Helsinki

Location of printing Helsinki

Year 2017

Pages 170

urn <http://urn.fi/URN:ISBN:978-952-60-7411-5>

Tekijä

Saara Tuurala

Väitöskirjan nimi

Painetut entsyymattiset glukoosi/ilma paristot: suorituskyky, stabiilisuus ja massatuotanto

Julkaisija Kemian tekniikan korkeakoulu**Yksikkö** Kemian ja materiaalitieteen laitos**Sarja** Aalto University publication series DOCTORAL DISSERTATIONS 83/2017**Tutkimusala** Kemia**Käsikirjoituksen pvm** 13.01.2017**Väitöspäivä** 19.05.2017**Julkaisuluvan myöntämispäivä** 20.03.2017**Kieli** Englanti **Monografia** **Artikkeliväitöskirja** **Esseeväitöskirja****Tiivistelmä**

Entsyymattinen biopolttokenno (EBPK) muuntaa biopolttoaineen kemiallisen energian sähköksi biosähkökemiallisten reaktioiden avulla. Entsyymien käyttö metallikatalyyttien sijaan tuo monia etuja mm. uusiutuvuuden ja myrkyttömyyden. Entsyymit ovat kuitenkin varsin herkkiä muutoksille lämpötilassa, pH:ssa ja kosteudessa. Tästä syystä entsyymit tyypillisesti immobilisoidaan elektrodeihin joko kemiallisen tai fysikaalisen adsorption avulla. Elektrodit useimmiten upotetaan nestekennoon, joka sisältää optimaalisen elektrolyytin. Näin ollen tavanomaisen EBPK:n kokoonpano ei ole käytännöllinen, mistä syystä kehitettiin uudenlainen EBPK-rakenne.

Tässä työssä painettiin silkkipainotekniikalla entsyymattisia elektrodeja (4-12 cm²) paperipohjaisille alustoille luoden ohuita (n. 1 mm) ja taipuisia EBPK:ja. Työn tuloksena saatiin massatuotettava glukoosi/ilma bioparisto, joka voidaan säilyttää kuivana ja aktivoida tarpeen tullen puskuriliuksella. Bioparistojen teho on μW-luokkaa, mutta useita parannusmahdollisuuksia tehon suurentamiseksi on esitelty tässä työssä. Bioparisto voisi soveltua esim. matalatehoisten sensorien, RFID-tunnisteiden tai jopa iholle asetettavien kosmeettisten/lääkinnällisten lappujen virtalähteiksi.

Anodientsyymeinä tutkittiin kaupallista glukoosioksidaasia (GOx) sekä VTT:llä tuotettua aldoosidehydrogenaasia (ALDH). Katodientsyymeinä tutkittiin kahta VTT:llä tuotettua lakkaasia, joista ensimmäisen alkuperä on *Trametes hirsuta* (ThL) ja toisen *Melanocarpus albomyces*. Näiden lisäksi tutkittiin teollista lakkaasia (EcoL). Menetelmät pitivät sisällään musteiden valmistusta erilaisten hiilien, biohteensopivien sidosaineiden ja entsyymi-mediaattori -parien avulla. Ensimmäiset painokokeet suoritettiin laboratoriossa käyttäen eri entsyymi-mediaattori -pareja sekoitettuna kaupalliseen hiilipohjaiseen musteseen. Tämän jälkeen tuotanto laajennettiin käyttäen GOx ja EcoL entsyymejä yhdessä VTT:llä tuotettujen grafiittipohjaisten musteiden kanssa. Painetut EBPK:t karakterisoitiin pääsääntöisesti sähkökemiallisia tekniikoita käyttäen.

Paras laboratoriossa saavutettu tehoteho ($P_{\max} = 3.5 \mu\text{W cm}^{-2}$) saatiin ALDH/ThL-kennolla, jonka avoimenpiirinjännite (OCV) oli 0.62 V ja enimmäisenergia (E) n. 10 $\mu\text{Wh cm}^{-2}$. Parhaan GOx/ThL-kennon OCV oli 0.38 V, $P_{\max} = 1.4 \mu\text{W cm}^{-2}$ ja $E = 5.5 \mu\text{Wh cm}^{-2}$. Koe-erässä tuotettujen kennojen suorituskyky oli 50-90 % alhaisempi, koska käytetyt musteseokset olivat erilaiset sekä entsyymi-mediaattori -parien ikääntyminen kiihtyi kohotetun kuivatuslämpötilan (23 °C v. 70 °C) ja pidennetyn säilytyksen (yksi päivä v. yksi viikko) vuoksi. Painettujen entsyymien (GOx ja EcoL) stabiilisuus oli hyvä, sillä ne menettivät korkeintaan 40 % aktiivisuudestaan kuivatus- ja säilytyslämpötilasta riippumatta. Mediaattorien lisääminen musteisiin kiihdytti entsyymien ikääntymistä, ja 70-80 % aktiivisuudesta oli menetetty kuukauden säilytyksen aikana. Anodi todettiin olevan rajoittava tekijä, minkä vuoksi erilaisia tapoja testattiin anodin suorituskyvyn parantamiseksi.

Avainsanat entsyymattinen biopolttokenno, entsyymattiset elektrodit, bioparisto, silkkipainatus**ISBN (painettu)** 978-952-60-7412-2**ISBN (pdf)** 978-952-60-7411-5**ISSN-L** 1799-4934**ISSN (painettu)** 1799-4934**ISSN (pdf)** 1799-4942**Julkaisupaikka** Helsinki**Painopaikka** Helsinki**Vuosi** 2017**Sivumäärä** 170**urn** http://urn.fi/URN:ISBN:978-952-60-7411-5

Preface

The research presented in this thesis was carried out in the research team of Printed Sensors and Electronic Devices at the VTT Technical Research Centre of Finland (VTT) during the period 2009-2015. The work was part of two national projects, funded by the Finnish Funding Agency for Innovation (Tekes). I also received a personal grant from VTT for writing the thesis. The thesis was finalised during my study leave and I am grateful to the Finnish Education Fund for supporting me financially with an adult education allowance. This thesis was academically approved at the School of Chemical Engineering at Aalto University (formerly Helsinki University of Technology).

First of all, I want to thank my professor Lasse Murtomäki for the opportunity to be a part time doctoral student under his supervision. I am also grateful to my advisors Associate Professor Tanja Kallio and Research Team Leader Dr Maria Smolander for your guidance and advice throughout the work. This thesis work included a lot of practical work and I want to thank my colleagues Anu Vaari, Asta Pesonen and Kaisa Kiri for your help in that. Colleagues Harry Boer and Anu Koivula, thank you for your advice on the enzymes used in this thesis. Colleagues Otto-Ville Kaukoniemi and Tiina Maaninen, thank you for your contribution in the pilot scale manufacturing process. I also want to thank my former colleagues Matti Valkiainen, Johanna Uotila, Leo von Hertzen and Jari Keskinen for your contributions to this work. I am also grateful to Mikael Bergelin, Jan-Erik Eriksson and Pia Sjöberg from Åbo Akademi and to Peter Jenkins for your advice in the bioelectrochemical part of this work and for helping me with my publications. My office roommates Marja Vilkmán and Reetta Grenman, thank you for your support and humour.

I want to thank Professor Shelley D. Minteer and Professor Plamen Atanassov for the opportunity to visit your laboratories and learn about enzyme immobilisation and paper-based biofuel cells. Stephanie Maltzman, Stephanie Bortz, Zana Brower, Nina Zulic Hausmann, Lindsey Pelster, Carolin Schneider-Lau, Kyle Sjöholm, Claudia Narváez Villarrubia, Omar Garcia, Jared Roy, Michael Moehlenbrock, Rob Arechederra, Lisa Palmer, Marja Murray, Gustavo Ciniciato - thank you for your friendship, I felt like home because of you.

I would also like to express my sincere gratitude to my pre-examiners Associate Professor Scott Calabrese Barton and Reader Daren Caruana for your constructive comments and analysis. I was able to improve my thesis through your contribution.

In addition to academic support, I am grateful for my dear friends. Thank you for your endless support and for helping me enjoy life outside work. Niina Hagman and Frank Russi, Maija and Tuukka Heikinheimo, Jenni Antikainen and Markku Laine, Miiia and Toni Fohlin, Johanna Metsomaa and Kalle Anttila, Ulpu Remes, Katriina Valkeapää, Helinä Pohjanlehto, Sanna Keskiöja, Tanja and Mikko Noranta, Ville Aarnikko, Teemu Lohenoja - I would not have made it without you.

Finally, to my whole family - thank you for your support throughout my whole life. Thank you Auli and Jyrki Pirttikoski for being great parents and my younger siblings Henri, Kasper and Matleena for being there. To my pillar of strength Erik Goussev - you have been the one who secured my way all the way to the top.

Helsinki, April 24, 2017,

Saara Tuurala

List of publications

This thesis is based on the following original publications, which are referred to in the text as I–VI. The publications are reproduced with kind permission from the publishers.

- I **Tuurala, S.**, Lau, C., Atanassov, P., Smolander, M., and Minteer, S.D. (2012) Characterization and Stability Study of Immobilized PQQ-Dependent Aldose Dehydrogenase Bioanodes. *Electroanalysis* 24(2), 229-238.
- II Jenkins, P., **Tuurala, S.**, Vaari, A., Valkiainen, M., Smolander, M., and Leech, D. (2012) A comparison of glucose oxidase and aldose dehydrogenase as mediated anodes in printed glucose/oxygen enzymatic fuel cells using ABTS/laccase cathodes. *Bioelectrochemistry* 87, 172-177.
- III Jenkins, P., **Tuurala, S.**, Vaari, A., Valkiainen, M., Smolander, M., and Leech, D. (2012) A mediated glucose/oxygen enzymatic fuel cell based on printed carbon inks containing aldose dehydrogenase and laccase as anode and cathode. *Enzyme and microbial technology* 50(3), 181-187.
- IV **Tuurala, S.**, Kaukoniemi, O.V., von Hertzen, L., Uotila, J., Vaari, A., Bergelin, M., Sjöberg, P., Eriksson, J.E., and Smolander, M. (2014) Scale-up of manufacturing of printed enzyme electrodes for enzymatic power source applications. *Journal of Applied Electrochemistry* 44(7), 881-892.
- V **Tuurala, S.**, Kallio, T., Smolander, M., and Bergelin, M. (2015) Increasing performance and stability of mass-manufacturable biobatteries by ink modification. *Sensing and Bio-Sensing Research* 4, 61-69.
- VI **Tuurala, S.**, Kallio, T., Smolander, M., and Bergelin, M. (2015) Increasing operational lifetime of printed enzymatic power sources using superabsorbent polymers as anode support. *Energy Technology* 3, 1080-1083.

Author's contributions

Publication I Saara Tuurala conducted the study plan, electrochemical measurements and data analysis, and was the main author of the publication. The SEM imaging was conducted by Dr Carolin Lau.

Publication II Saara Tuurala prepared the enzymatic inks, assembled the biofuel cells and conducted the electrochemical characterisation of the cells together with the first co-author. Saara Tuurala took an active part in the data analysis and writing of the publication. The synthesis of the mediators and the solution phase studies were conducted by Dr Peter Jenkins.

Publication III Saara Tuurala prepared the enzymatic inks, assembled the biofuel cells and conducted the electrochemical characterisation of the cells together with the first co-author. Saara Tuurala took an active part in the data analysis and writing of the publication. The synthesis of the mediators and the solution phase studies were conducted by Dr Peter Jenkins.

Publication IV Saara Tuurala planned the electrochemical measurements and enzyme stability study of printed enzyme electrodes. Saara Tuurala carried out all the electrochemical measurements and data analysis related to them, as well as data analysis of the enzyme stability and microscopy study of printed enzymatic electrodes. Saara Tuurala took an active part in the development of the enzymatic inks. Saara Tuurala was the main author of the publication. The solution phase studies of enzyme-mediator pairs were conducted by Dr Mikael Bergelin and Dr Jan-Erik Eriksson. The base ink drying experiments for the roll-to-roll manufacturing were conducted by Leo von Hertzen. Dr Tiina Maaninen and Otto-Ville Kaukoniemi were in charge of the roll-to-roll manufacturing and Saara Tuurala took part in the printing process. The microscopy imaging of the printed electrodes was conducted by Dr Tiina Maaninen.

Publication V Saara Tuurala conducted the study plan, electrochemical measurements and data analysis, and was the main author of the publication. Dr Tiina Maaninen was in charge of the roll-to-roll manufacturing. The microscopy imaging of the printed electrodes was conducted by Dr Tiina Maaninen.

Publication VI Saara Tuurala conducted the study plan, electrochemical measurements and data analysis, and was the main author of the publication.

Contents

Preface	3
List of publications	6
Author's contributions	7
Abbreviations and symbols	10
1. Introduction	13
1.1 Motivation - Why an enzymatic biofuel cell?.....	13
1.2 Objective - From liquid phase biofuel cell to printed thin biobattery.....	14
1.3 Progression - From laboratory to pilot scale manufacturing.....	14
2. The glucose/air biofuel cell	16
2.1 Enzymes as catalysts.....	16
2.1.1 Enzyme kinetics.....	17
2.1.2 Anode enzymes for glucose oxidation.....	18
2.1.3 Cathode enzymes for oxygen reduction.....	20
2.2 Electron transfer from enzyme to the electrode.....	21
2.2.1 Direct electron transfer.....	21
2.2.2 Mediated electron transfer.....	22
2.3 Potential losses in EBFC.....	23
2.4 Mass transport in EBFC.....	24
3. Experimental methods	25
3.1 Manufacturing methods.....	25
3.1.1 Immobilisation and stabilisation of enzymes.....	25
3.1.2 Preparation of enzymatic inks.....	25
3.1.3 Printing process of enzymatic electrodes.....	26
3.2 Morphology of electrodes.....	28
3.3 Enzyme activity measurements of printed electrodes.....	28
3.4 Cell assemblies.....	28
3.4.1 Liquid cell.....	28
3.4.2 Stand-alone cell.....	29
3.4.3 Pd/H ₂ reference electrode cell.....	29
3.4.4 Cardboard cell.....	30
3.5 Electrochemical methods.....	31
3.5.1 Voltammetric measurements.....	31
3.5.2 Potentiometric measurements.....	32
3.5.3 Amperometric measurements.....	33
3.5.4 Coulometric measurements.....	33
4. Research contribution	34
4.1 Immobilized ALDH Bioanodes (Publication I).....	34
4.2 Printed mediated ALDH/ThL EBFCs (Publications II and III).....	35

4.3	Scale-up of manufacturing (Publication IV)	39
4.4	Increasing the performance of the GOx/FcMeOH anode (Publication V)	41
4.5	SAPs as anode support (Publication VI)	42
4.6	Further improvements of enzymatic inks	43
4.6.1	Increase of anode performance by increasing GOx/FcMeOH in the ink and changing the substrate to carbon fibre paper	43
4.6.2	Changing graphite to carbon black in enzymatic inks	44
5.	Discussion	47
5.1	Performance	47
5.2	Stability	48
5.3	Mass-manufacturing	49
5.4	Comparison to other flexible EBFCs	50
5.5	Suggestions for future research and development	53
6.	Summary and conclusions	54
	Bibliography	55

Appendices

Appendix A: Electron transfer properties of ferro/ferricyanide on DuPont ink

Appendix B: Studying DET of ThL and rMaL in a fuel cell setup

Appendix C: A stack of biobatteries combined with printed supercapacitors

Publications I–VI

Abbreviations and symbols

List of abbreviations

ABTS	2,2'-azino-bis(3-ethylbenzothiazoline-6-sulfonic acid) di-ammonium salt
ABTS ⁺	first oxidation state of ABTS
ABTS ²⁺	second oxidation state of ABTS
ALDH	aldose dehydrogenase
BFC	biofuel cell
BOD	bilirubin oxidase
CA	chronoamperometry
CB	carbon black
CMC	carboxymethyl cellulose
CP	chronopotentiometry
CV	cyclic voltammetry
DET	direct electron transfer
EBFC	enzymatic biofuel cell
EcoL	Ecostone laccase
FAD	flavin adenine dinucleotide
FADH ₂	reduced form of FAD
FcMeOH	ferrocenemethanol
FDH	fructose dehydrogenase
GDH	glucose dehydrogenase
GOx	glucose oxidase
iV-curve	polarisation curve
L-cell	liquid cell

LOx	lactate oxidase
MaL	<i>Melanocarpus albomyces</i> laccase
MET	mediated electron transfer
mGDH	membrane-bound GDH
MWCNT	multi-walled carbon nanotube
NHE	normal hydrogen electrode
OCV	open circuit voltage
ORR	oxygen reduction reaction
pI	isoelectric point
Pd/H ₂	palladium-hydrogen
PEO	polyethylene oxide
PQQ	pyrroloquinoline quinone
PQQH ₂	reduced form of PQQ
R2R	roll-to-roll
RFID	radio-frequency identification
rMaL	recombinant MaL
SAP	superabsorbent polymer
SEM	scanning electron microscopy
sGDH	soluble GDH
TBAB	tetrabutylammonium bromide
ThL	<i>Trametes hirsuta</i> laccase
TMPD	<i>N,N,N',N'</i> -tetramethyl- <i>p</i> -phenylenediamine

List of symbols

A	area
c	concentration
D	diffusion coefficient
E	electric potential
E	energy density
E^0	formal potential
E_a	anodic potential
E_c	cathodic potential
$E_{\text{cut-off}}$	cut-off potential
F	Faraday constant
I	current
K_m	Michaelis-Menten constant
K_S	dissociation constant
k	reaction rate constant
n	number of electrons
R	gas constant
T	temperature
Q	charge density
v	scan rate
v_0	reaction rate
V_{max}	maximum reaction rate

1. Introduction

1.1 Motivation - Why an enzymatic biofuel cell?

As portable and wearable electronics become more and more common in our everyday lives, there is a clear need for flexible and sustainable power sources. Electronics are planned to be integrated into e.g. household devices, clothing and even the human body, and they need to be almost indistinguishable, meaning in practice as thin, flexible and disposable as possible.

Although current battery chemistries (e.g. Zn/MnO₂, Zn/air and Li-ion) are being converted from their solid form to printed flexible platforms (see e.g. [1]–[5]), they still face many challenges. First of all, the use of metals as active materials introduces issues of disposability, toxicity and availability. In addition, the need for a specific electrolyte between the anode and cathode layers affects the manufacturing process as well as the shelf-life. Applying and sealing of a moist electrolyte between the anode and cathode is a demanding manufacturing step. If the electrolyte leaks out from the cell during storage, the cells soon become dry and lose their functionality. Hence, there is a need for alternative, environmentally friendly battery configurations.

For the reasons outlined above, a new type of printed battery was developed in this thesis. This battery uses enzymes as catalysts and converts the chemical energy of biofuel into electrical energy. The fuel at the anode is sugar and that at the cathode is oxygen from air. The use of enzymes as catalysts confers many advantages over metal catalysts: 1) they are renewable, 2) they operate in mild conditions, 3) they have no toxicity issues, and 4) they can selectively oxidise different renewable fuels (e.g. sugars and alcohols).

Research on enzymes as biocatalysts in biofuel cells (BFC) began in the early 1960s, and the first enzymatic BFC (EBFC) was produced in 1964 [6]. EBFCs were first studied by NASA in order to find ways to recycle human waste into usable energy in space crafts. However, due to poor performance and stability the research was not active until 1980s, when researchers started to study methanol oxidation by enzymes. In 1998 Palmore et al. [7] demonstrated complete oxidation of methanol to CO₂ by enzymatic cascade. Since then, the group led by Shelley Minteer has developed immobilised enzyme cascade electrodes for full oxidation of methanol, ethanol, glycerol, lactate and sugar to carbon dioxide in an EBFC [8]–[12]. Through electrical wiring of enzymes, Adam Heller's group demonstrated a miniaturised glucose/air EBFC operating in a grapefruit [13]–[15]. The group led by Evgeny Katz has demonstrated the operation of EBFCs e.g. in living clams and a snail as well as operation of a pacemaker powered by an implantable EBFC [16]–[18]. In addition, self-powered electrochemical devices utilising EBFCs have been developed, such as biosensors, memristors, and immunoassays [19]–[21]. Hence, the three main applications for EBFCs are implantable BFCs, self-powered sensors, and power supplies for small portable and wearable power devices [22]–[25]. The greatest challenges facing EBFC-based technology are their rather poor power generation and stability,

and bulky design [26]. These three aspects were studied in this thesis by developing enzymatic inks and assembling EBFCs using printed enzymatic electrodes. The printing process of these inks was first demonstrated in the laboratory and then scaled up to pilot scale manufacture.

1.2 Objective - From liquid phase biofuel cell to printed thin biobattery

The most common type of EBFC contains a liquid chamber into which both anode and cathode electrodes are inserted (Figure 1a). Optimally, the anode and cathode enzymes are fully immobilised into the electrode structures and no separator is needed due to the high selectivity of enzymes. However, typically an ion exchange membrane is needed to prevent anode and cathode chemicals from mixing together.

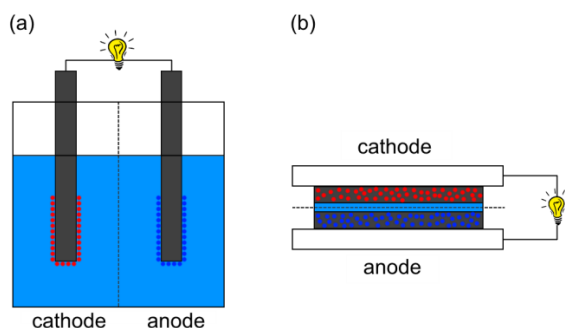


Figure 1. (a) Schematic of a conventional liquid-chamber EBFC. The electrodes consist of graphite rods on which the anode and cathode enzymes are immobilised. (b) Schematic of a planar EBFC. The electrodes are manufactured by printing enzymatic carbon-based inks on an electrically conductive substrate. The immobilised anode and cathode enzymes are represented as blue and red spheres, respectively.

In order to make EBFCs portable and easy to integrate for thin applications, the conventional structure needs to be changed. By mimicking a planar fuel cell structure and producing enzymatic electrodes by a printing process, a layered EBFC configuration was created (Figure 1b). Although this design miniaturises the cell structure, as well as simplifying the manufacturing process, it still faces many challenges, mainly related to enzyme stability and functionality. Hence, the objective of this thesis was to develop a printable, stable and scalable biobattery that can be stored dry and activated on demand. The main research questions were:

- How to develop enzyme-containing inks? (Publications I-V)
- What affects the performance and stability of printed electrodes? (Publications I-VI)
- Is it possible to demonstrate their production by printing in pilot scale? (Publications IV and V)

1.3 Progression - From laboratory to pilot scale manufacturing

As the main challenge when working with enzymes is their stability, they need to be protected against changes in temperature, pH and moisture. Immobilisation is a way to maintain the 3D structure of an enzyme

and thus its activity. Immobilisation can increase the molecular rigidity of an enzyme as well as create a protected microenvironment. There are many types of immobilisation techniques, such as covalent attachment or physical adsorption to a support, entrapment in a matrix or cross-linking of an enzyme [27]–[30], and the best immobilisation strategy is enzyme-specific. Consequently, the first task of this work was to study different polymer structures for immobilising and stabilising a very sensitive anode enzyme (Publication I).

Another challenge related to BFCs is their relatively poor electrochemical performance. This can be optimised by selecting the most suitable mediator molecules for shuttling electrons between the active site of the enzyme and the electrode surface. The use of osmium-based redox complexes as optional mediator molecules was investigated in printable enzyme electrodes, and fully printable BFCs were manufactured (Publications II and III).

As the printing process of enzyme electrodes was demonstrated to be successful in laboratory screen-printing, the next challenge was to scale up the printing process to a roll-to-roll (R2R) pilot scale. As there are many process steps in R2R manufacturing, including rotary screen-printing and drying of inks, they needed to be investigated (Publication IV). As a result, the printing process was scaled up from laboratory to pilot scale, and functional enzyme-containing electrodes were manufactured.

Although scale-up was successfully achieved, there were still challenges concerning the anode stability. For this reason, the anode-ink was reformulated in order to achieve better mechanical and functional stability (Publication V). As the last optimisation and stabilisation approach, a glue-like biocompatible polymer was introduced into the anode as a supporting element (Publication VI).

The outcome of this thesis work is a single-use, disposable and moisture-activated thin biobattery for μ -power applications, which can be manufactured on an industrial scale. The work flow of the whole thesis work is illustrated in Figure 2.

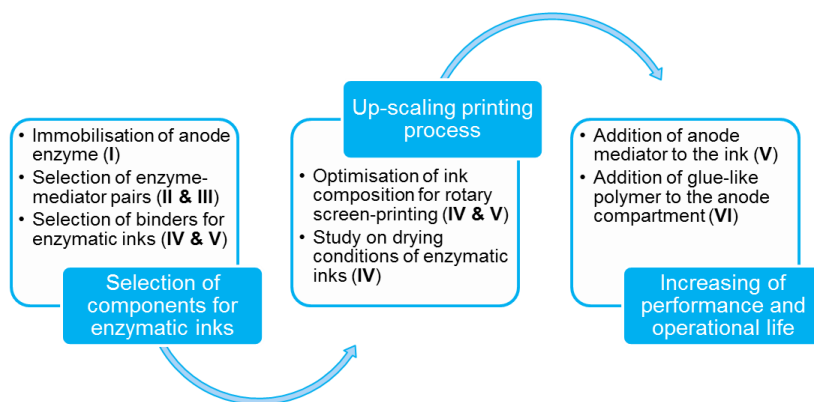


Figure 2. Progression of the thesis work.

2. The glucose/air biofuel cell

Any BFC is a fuel cell that contains biological catalysts [31]. Typically, the biocatalysts used are microorganisms or enzymes [32]. The operational principle of an EBFC [33], [34], using glucose and oxygen as fuel, is illustrated in Figure 3. On the anode, glucose is oxidised by an enzyme to gluconolactone, and on the cathode, oxygen is reduced by another enzyme to water, as shown in Equations (1) and (2).

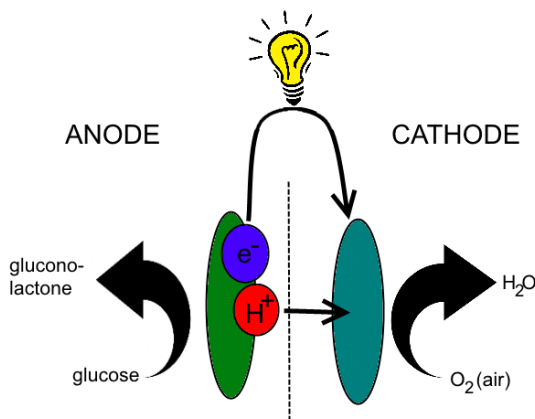
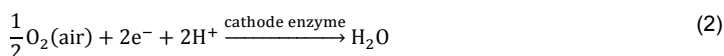
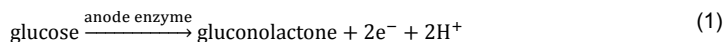


Figure 3. Illustration of the operational principle of a glucose/air EBFC.



2.1 Enzymes as catalysts

Most metal catalysts catalyse a wide range of reactions, and hence they are usually not very selective. By contrast, enzymes are often highly selective, catalysing only very specific reactions. Enzymes lower the activation energy of certain biochemical reactions by providing an alternative reaction pathway. Enzymes take part in the reaction but they do not undergo permanent changes. In common with other catalysts, enzymes can only alter the rate of reaction, not the reaction equilibrium. [35]

Some enzymes consist of a protein and a cofactor, which is a chemical compound required for the protein's biological activity. Cofactors can be either organic or inorganic. Organic cofactors may be tightly or even covalently bound to the enzyme (e.g. flavin); they are called prosthetic groups. Organic molecules which are not permanently bound to the enzyme, but are involved directly in an enzyme-catalysed reaction (e.g. vitamin C) and combine temporarily with the enzyme-substrate complex, are called coenzymes. It must be mentioned, however, that this terminology can be slightly different in different sources [36]. Inorganic

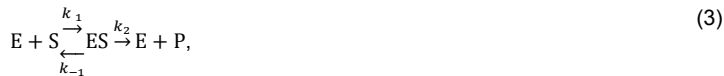
cofactors are usually positively charged metal ions (e.g. Fe^{2+} , Mg^{2+} or Zn^{2+}) which bind temporarily to the active site of the enzyme, giving an intense local positive charge to the protein. Some enzymes or enzyme complexes require several cofactors, and in many cases the cofactor includes both an organic and an inorganic component (e.g. heme).

Enzyme proteins are often spherical, and in order to catalyse their reactions they must maintain their secondary and tertiary structures [37]. The intra- and intermolecular bonds that stabilise a protein structure are disrupted by changes in temperature, pH and hydration, which affects the overall conformation and thus the catalytic activity of the enzyme. Enzyme activity can also be affected by other molecules. Inhibitors and activators are molecules that decrease and increase enzyme activity, respectively, by binding to the active site of the enzyme.

In order to generate electricity, the selected enzymes need to be oxidoreductases due to their ability to catalyse electron transfer from one molecule to another. For comparison, transferases enact the transfer of specific functional groups from one molecule to another, and no electricity can be harvested. Many redox enzymes catalyse reactions at potentials that are close to the theoretical oxidation or reduction potentials of their substrates. This is most suitable for power sources because a high cell potential is needed for high power output. As an example, at pH 7 the theoretical oxidation potential of glucose is -0.42 V and the theoretical reduction potential of oxygen is 0.82 V, which would generate a cell potential of 1.24 V. Other characteristics needed from enzymes for power source applications are high turnover of the substrate (activity), stability and availability. These characteristics must be taken into account when large-scale manufacturing of biobatteries is planned.

2.1.1 Enzyme kinetics

During catalysis, an enzyme substrate (ES) complex is formed by binding the substrate (S) into the active site of the enzyme (E), finally resulting in a reaction product (P). The stability of the ES is related to the affinity of the substrate for the particular enzyme, and is characterized by its dissociation constant, K_s , for the ES complex:



$$K_s = \frac{k_{-1} + k_2}{k_1}, \quad (4)$$

where k 's are the reaction rate constants for each individual reaction. As $k_2 \gg k_{-1}$, the term k_2 is referred to as the catalytic rate constant or turnover number, k_{cat} (typically in the order of 10^3 s^{-1}), and K_s is called the Michaelis-Menten constant, K_m . The overall rate of formation of P is given by the Michaelis-Menten equation:

$$[\text{E}_0] = [\text{E}] + [\text{ES}], \quad (5)$$

$$v_0 = \frac{k_{\text{cat}}[\text{E}_0][\text{S}]}{[\text{S}] + K_m} = \frac{V_{\text{max}}[\text{S}]}{K_m + [\text{S}]} \quad (6)$$

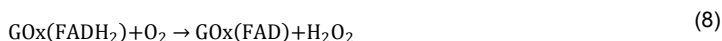
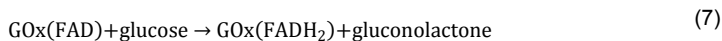
where maximum reaction rate, V_{max} , is achieved when all of the available enzymes are bound with the substrate.

2.1.2 Anode enzymes for glucose oxidation

There are two main groups of enzymes that use glucose as their principal substrate: glucose oxidases (GOx) and glucose dehydrogenases (GDH). The category depends on the enzyme's ability to react with external electron acceptors. GOxs are defined as oxidoreductases that can utilize oxygen as the external electron acceptor, whereas GDHs are defined as oxidoreductases that are unable to utilize oxygen as the electron acceptor and instead transfer electrons to various natural and artificial electron acceptors [38].

GOxs are generally very stable and available enzymes, which have their cofactor tightly bound in the protein but show low activity. GDHs on the other hand have high turnover of their substrate, but they may require a soluble cofactor and are typically unstable [38], [39]. Hence, from the point of view of a power source, the two enzyme groups have both advantageous and disadvantageous characteristics. For this reason, both commercial GOx and in-house purified GDH-like enzymes were tested as anode enzymes in EBFC.

Glucose oxidase (EC 1.1.3.4) catalyses specifically the oxidation of β -D-glucose to D-glucono- δ -lactone and hydrogen peroxide (H_2O_2), as shown in Equations (7) and (8). The reaction mechanism is based on a concert transfer of a proton from glucose to a basic group on the enzyme and a direct hydride transfer from glucose to the cofactor [40], [41]. The cofactor of GOx is flavin adenine dinucleotide (FAD), which is tightly bound to the protein; hence it is a prosthetic group. FAD works as the initial electron acceptor and is reduced to $FADH_2$, after which it is oxidised back to FAD by the final electron acceptor, molecular oxygen, which is reduced to H_2O_2 . The redox potential of free FAD is -0.22 V vs. normal hydrogen electrode (NHE) and the redox reaction of FAD-GOx occurs at around -0.2 V vs. NHE [42]–[45]. The reduction potential of O_2 to H_2O_2 is 0.29 V vs. NHE at pH 7.



GOx is found in several species of fungi and insects (e.g. honeybee) and functions as an antibacterial substance in nature by killing bacteria with H_2O_2 . GOx is often extracted from *Aspergillus niger*, a fungus which causes black mould on certain fruits and vegetables and is commercially available at a reasonable price.

GOx is a homodimer with an average diameter of 8 nm and molecular mass between 150-180 kDa, typically 160 kDa. The isoelectric point (pI) of GOx is around pH 4 (see e.g. Wilson and Turner [39] and references therein). The substrate-binding domain of GOx is characterised by a deep pocket with FAD located on its base [46]; hence the substrate and oxygen must transfer deep into the enzyme in order to become oxidised and reduced, respectively. The crystal structure of GOx is shown in Figure 4.

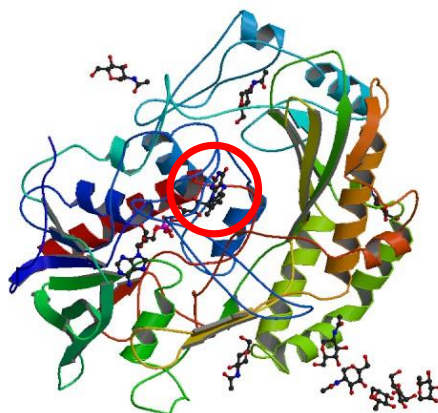
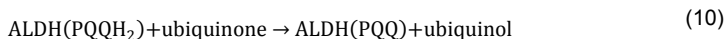
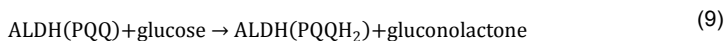


Figure 4. Crystal structure of monomeric GOx enzyme from *Aspergillus niger*. FAD is shown as a ball-and-stick representation inside the protein (circled in red). Protein chains are coloured from the N-terminus (green) to the C-terminus (blue) using a rainbow colour gradient. Image from the RCSB PDB (www.rcsb.org) of PDB ID 1GAL, original data from Hecht et al. [46].

Quinoprotein GDH (EC 1.1.5.2) refers to at least two distinct groups of GDHs harbouring pyrroloquinoline quinone (PQQ) as the redox cofactor: membrane-bound PQQ-GDH (mGDH) and water-soluble PQQ-GDH (sGDH). mGDHs have been reported from a variety of Gram-negative bacteria, and their substrate specificity, stability, and other features are strain-specific [38]. The physiological role of mGDH, coupled with the respiratory chain via ubiquinone, is the terminal oxidation of glucose.

Aldose dehydrogenase (ALDH) from Gram-negative *Gluconobacter oxydans* is a membrane-bound protein which can oxidise aldose sugars, e.g. glucose and xylose [47]. Like mGDH, ALDH has a prosthetic group PQQ which is the initial electron acceptor in the oxidising reaction of glucose, and ubiquinone is the natural electron acceptor as shown in Equations (9) and (10). The electrochemistry of both free PQQ and PQQ-GDHs is still poorly understood, but it is known that the reduction of PQQ takes place in two one-electron steps forming a semi-quinone between the fully oxidised and reduced forms. The reaction mechanism is assumed to proceed by base-catalysed hydride transfer, as in the case of GOx [48]–[50]. Because PQQ is very sensitive to pH and temperature, possessing at least five pK_as [51], the redox potentials for PQQ-GDHs are widely spread between ca. 0.005 and 0.105 V, being typically 0.09 V [52]–[55]. The redox potential of ubiquinone is 0.045 V vs. NHE at pH 7.



The main advantage of using quinoproteins in power source applications is their typical insensitivity to oxygen and hence no H₂O₂ is formed in the reaction. However, O₂ has been reported to act as an electron

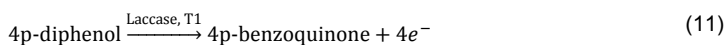
acceptor for mGDHs in basic medium, which is probably due to unique properties of the active site of mGDH. At neutral pH and in the presence of a suitable artificial electron acceptor, O₂ is not consumed [56].

mGDHs are partly homologous to other PQQ-dependent enzymes (except sGDH), notably to amino acid residues surrounding PQQ. Hence, the structure of ALDH can be expected to follow the common tertiary structure of PQQ-dependent enzymes [48], [49], [57]. Like other mGDHs, ALDH has a molecular mass of 87 kDa and is a monomeric enzyme [47]. The pI of mGDH from *Gluconobacter suboxydans* is 7.8 [58], and it is probably the same enzyme as ALDH [47]. Hence ALDH is a more basic enzyme than GOx.

2.1.3 Cathode enzymes for oxygen reduction

In a glucose/air EBFC, the reduction of dissolved or atmospheric O₂ to water at the cathode occurs via four proton – four electron transfer (oxygen reduction reaction, ORR). The achievement of a low-overpotential ORR at pH close to neutral is one of the most difficult electrocatalytic reactions in the field of small substrate activation. Whereas most metal catalysts require high overpotentials, multi-copper oxidases, such as laccases and bilirubin oxidases (BOD), have demonstrated low-overpotential ORR at close to neutral pH and for this reason the study of enzymatic cathodes has focused mainly on laccases and BODs (see e.g. [59]–[63]). In this thesis, laccases were selected as the cathode enzyme due to VTT's in-house expertise in their production and characterisation.

Laccases (EC 1.10.3.2) belong to a group of polyphenol oxidases containing four copper atoms in the catalytic centre (Figure 5a). Laccases catalyse ORR to water, accompanied by the oxidation of a substrate, typically p-diphenol or other phenolic compounds, as shown in Equations (11) and (12). As oxygen is usually present in their environment, laccases do not need the addition or synthesis of a low molecular weight co-factor.



Laccases have two separate copper sites: a mononuclear site (T1 copper ion) and a trinuclear site that is a cluster of T2, T3, and T3' copper ions (Figure 5). Reducing substrates are oxidized close to the mononuclear site due to its high redox potential of ca. 790 mV vs. NHE, although the potential of the T1 Cu sites varies between laccases. Electrons are then transferred through a Cys-His pathway into the trinuclear site where O₂ is reduced to water at around 400 mV vs. NHE. Although the copper-binding site arrangement into domains varies remarkably between different laccases, the geometries of the copper sites are very similar [64]. Typically, the molecular weight of fungal laccases is 60-70 kDa and their pI is ca. 4.0 [65].

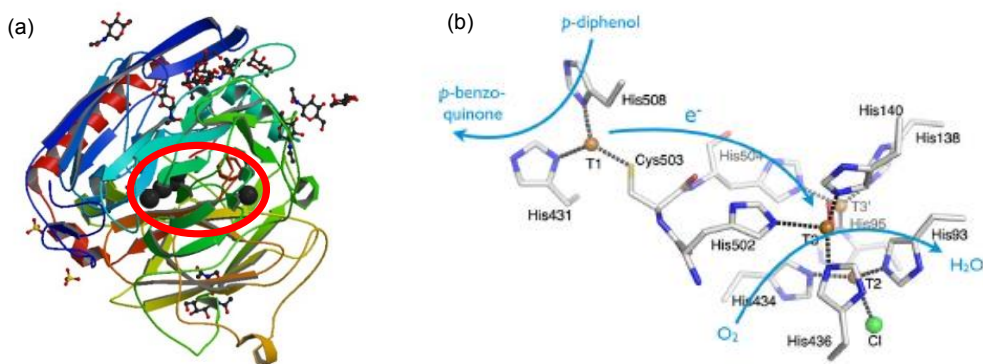


Figure 5. (a) Crystal structure of recombinant laccase from *Melanocarpus albomyces* (rMaL). Protein chains are coloured from the N-terminus (green) to the C-terminus (blue) using a rainbow colour gradient. The Cu-atoms are represented as black spheres, where T1 is closest to the outer layer of the protein and the T2/T3 trinuclear site is located inside the enzyme (circled in red). Image from the RCSB PDB (www.rcsb.org) of PDB ID 2IH8, original data from Hakulinen et al. [66]. (b) Copper sites as observed in MaL and the electron pathway. (Reprinted from [64] with permission.)

Laccases are typically found in plants and fungi (see e.g. [67], [68]). Their natural occurrence is related to e.g. degradation of biopolymers, detoxification and lignin polymerization (see e.g. [65], [69]). Most laccases are extracellular enzymes, which makes their purification procedures relatively easy. In addition, laccases generally exhibit a considerable level of stability in the extracellular environment, probably due to their high extent of glycosylation [70]. Nowadays laccases are widely used in different applications, e.g. in bio-bleaching, biological pulping, wine stabilisation, waste detoxification and decontamination (see e.g. [65], [67], [71] and references therein).

Three different laccases were used in this thesis. Two of them were produced in-house from *Trametes hirsuta* (ThL) and *Melanocarpus albomyces* (MaL, produced as a recombinant enzyme in the fungus *Trichoderma reesei*). ThL is considered to be a high potential laccase ($E^0 = 700\text{-}800\text{ mV}$), whereas MaL is a low potential laccase ($E^0 \leq 500\text{ mV}$). The two enzymes also have different pH optima: pH 3-5 for ThL and pH 4-7 for MaL depending on the substrate [59], [72]. One industrial laccase, Ecostone LCL 45 from AB Enzymes (EcoL), was used in the pilot manufacturing trials (Publications IV-VI).

2.2 Electron transfer from enzyme to the electrode

2.2.1 Direct electron transfer

In direct electron transfer (DET) the enzyme and current collector are in direct contact, and electrons pass from the electrode to the reducing redox centre of the enzyme. DET allows the use of the full thermodynamic potential of the enzyme, without the overpotential of electron transfer from the enzyme to a mediator. In bio-systems, electron transfer rates within and between species, as well as between electrodes and species in their proximity, decay exponentially with the distance between the involved centres. Kinetics measurements

have shown that electrons can tunnel about 25 Å through proteins in biologically relevant time scales [73], although the electron transfer rates drop by a factor of $\sim 10^4$ when the distance between an electron donor and an acceptor is increased from 8 to 17 Å [74].

PQQ-dependent, heme-containing and FAD-dependent enzymes can undergo DET. For example, DET of PQQ-dependent alcohol dehydrogenase and FAD-dependent GOx has been characterized and their anodic operation demonstrated in BFCs. However, reduced GOx does not directly transfer electrons to conventional electrodes (e.g. Au or glassy carbon), because the distance between its redox centres and the electrode surface exceeds the distance across which electrons are transferred at sufficient rates [75]. In addition, ALDH has been shown to perform DET but with very poor efficiency [76], probably due to the fact that it does not contain a heme group.

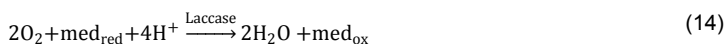
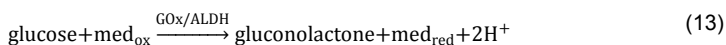
DET of laccase is possible if the enzyme is favourably oriented at the surface of the electrode. If laccase is successfully immobilized to the electrode, oxygen reduction bioelectrocatalysis can be achieved at the redox potential of the T1 copper active site, and hence oxygen can be reduced at low overpotentials, especially with high-potential laccases [63], [77], [78]. As an example, VTT's ThL has been shown to achieve DET on glassy carbon electrode by immobilizing laccase into a well-designed dual-layer architecture of PE-DOT₁ [79]. The ORR was achieved at 0.75 V vs. NHE at pH 4.5, which is close to the redox potential of the T1 Cu of ThL (0.78 V vs. NHE [59]).

2.2.2 Mediated electron transfer

In mediated electron transfer (MET), a redox-active molecule with reversible electron transfer properties is used to act as an electron shuttle between the electrode surface and the enzyme active site. The redox potential of the mediator must be close to the redox potential of the active site, but also ensure sufficient driving force for optimizing bioelectrocatalytic activity. A study by Gallaway and Calabrese Barton showed that the bimolecular rate constants for the mediator-laccase reaction are highly dependent on mediator potential [80]. If the potential difference between the laccase T1 Cu site and mediator (ΔE_{et}) exceeded 300 mV, no dependence of ΔE_{et} on the bimolecular rate constant was observed. For laccase of *T. versicolor* (formal potential, $E^0 = 0.82$ V), the optimum mediator potential was determined to be 0.66 V vs. NHE. Babanova et al. [52] studied quinone-modified surfaces with PQQ-GDH and indicated the optimal potential difference between the enzyme and mediator to be 148 ± 25 mV.

MET generally offers a higher current density than DET, if the mediator-enzyme system has been optimized. However, MET introduces an additional level of complexity, and electrode performance becomes a matter of mediator stability, as well its effect on the enzyme stability.

MET is compatible with almost all naturally occurring oxidoreductase enzymes and co-enzymes. In the case of glucose oxidation, mediator in its oxidised form is reduced by the anodic enzyme (GOx or ALDH). Next, the mediator transfers to the electrode surface and becomes oxidised again by releasing electrons (Equation (13)). In the case of ORR by laccase, mediator in its reduced form oxidizes by releasing electrons to the enzyme and transfers to the electrode surface to become reduced again (Equation (14)).



¹ poly(3,4-ethylenedioxythiophene)

2.3 Potential losses in EBFC

Although the theoretical potential of a glucose/air BFC is 1.24 V, this is rarely achieved in practice. This is due to overpotentials present in the cell. The most significant losses are the activation and reaction overpotentials due to slow electron transfer at the solid electrode surface and slow chemical reactions. Typically, enzyme co-factors have relatively high activation overpotentials, and for this reason glucose is oxidised at approximately 200 mV higher potentials than its theoretical potential. In the case of GOx and ALDH, the oxidation potentials of glucose are approximately at -0.2 and 0.1 V vs. NHE, respectively. In the case of laccases, activation overpotentials are significantly lower, because laccases do not have co-factors. As mediators are used to shuttle electrons between electrode surface and enzyme, the activation overpotential is even higher, and thus the cell potential lower. The cell potential generation is illustrated in Figure 6.

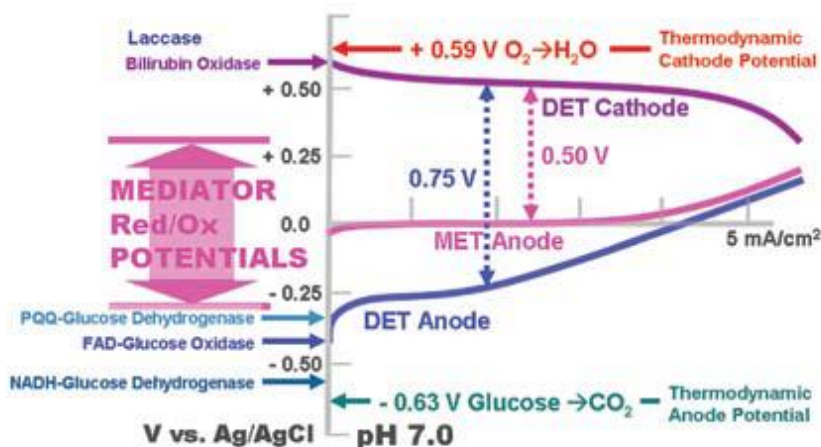


Figure 6. Principle of cell potential generation in an EBFC. The maximum oxidation potentials for glucose and the corresponding thermodynamic potential for ORR (pH 7) are indicated vs. Ag/AgCl reference electrode. Redox potentials of several enzymes and their corresponding co-factors are shown. (Reprinted from [22] with permission from The Electrochemical Society. Copyright 2007, The Electrochemical Society.)

Other losses in the electrode potential come from the ohmic resistance of the cell and the concentration overpotential. The former is attributed to cell design. It includes electrical conductivity of electrodes and current collectors, as well as proton conductivity between and through the electrolyte and the membrane. Concentration overpotential takes place at high current densities, when the transport of fuel and mediator into and out the enzymes, as well as the transport of a mediator from the enzyme to the electrode surface and back is too slow to maintain the reaction rate needed.

2.4 Mass transport in EBFC

Sufficient mass transport in an electrochemical cell is the key for high current densities. Efficient biocatalysis requires that both substrates and products freely diffuse inside and outside the immobilisation support. Enzyme immobilisation into polymers typically increases mass transfer limitations decreasing the reaction rate. Poor mass transfer can also aggravate product inhibition or induce undesirable pH gradients [30] leading to loss in enzymatic activity. High resistance for the mass transfer tends to build a concentration difference between the bulk phase and the sites of reaction, thus slowing down the reactions and leading to polarization of the electrodes. In the case of a mediated system, the mediator mass transport can have even higher impact on the reaction rate than enzyme kinetics [81].

In order to maximise power density, 3D electrodes have been developed. However, 3D electrodes are only valuable if they provide efficient mass transport. The presence of sufficient mass transport enables one to balance the overall effective surface area against porosity. This ensures that the maximum number of catalytic sites are available without suffering the blockage of fuel transport, which will be the case if the pore size is too small [33]. The electrodes should consist of multi-dimensional and multi-directional pores [34]. Multi-dimensionality provides both small pores to support enzyme stabilisation and high loading densities, and larger ones to support mass transport of liquid phase species. Multi-directionality provides higher surface area and permeability to liquid phase fuel transport, but it will eventually decrease structural strength if too extensive. It must be emphasised that the transport of the liquid phase species through a pore structure is only the first step; once the substrate has diffused to the enzyme surface, it must also cross an additional boundary layer that can also retard the mass transfer.

In the absence of assisted fluid flow, the mass transfer involves diffusion and migration [82]. Diffusion is the movement of ions and molecules due to concentration gradients whereas migration is the movement of charged species under the influence of a potential or electric field. Species subject to transport mechanisms in a mediated EBFC are fuels and reaction products; mediators both in oxidised and reduced forms; and buffer-electrolyte. Hence, multiple mass transfer processes both can be identified in a printed EBFC as illustrated in Figure 7.

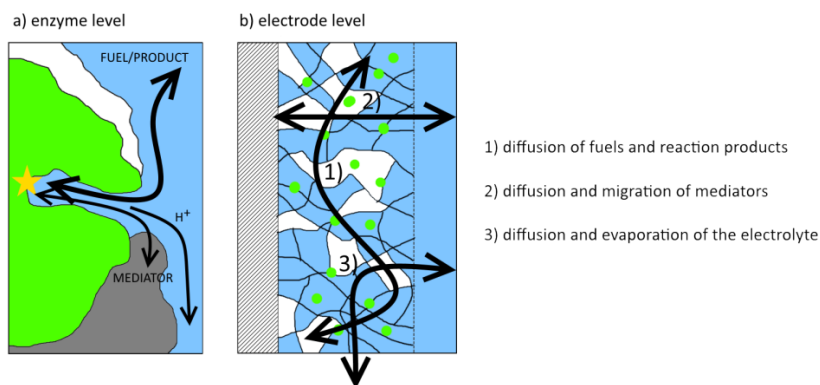


Figure 7. Schematic of different mass transport processes in a printed EBFC anode on a) enzyme level and b) electrode level. Enzymes (green), carbon support (grey, wires) and polymer (white) form the base of the electrode as they are immobilised.

3. Experimental methods

The first enzymatic anodes in this thesis were manufactured on carbon paper by drop-casting (Publication I). Printed enzymatic electrodes were manufactured by formulating inks and printing them on cellulose-based substrates (Publications II-V). Three different printing methods were used: rod-coating, laboratory scale screen printing and pilot scale rotary screen printing. The morphology of the printed electrodes was studied and their enzymatic activity was measured using various analytical techniques suitable for BFCs [83]. Most of the measurements conducted in this thesis were electrochemical measurements, including voltammetry, potentiometry, amperometry and coulometry.

Drop-casted bioanodes were characterized separately in a liquid phase cell (Publication I). Printed EBFCs were assembled using three different configurations. In the first configuration, printed electrodes were sandwiched between planar graphite current collectors (Publications II-V). In the second configuration, an inert reference electrode was inserted between the anode and cathode inside the separator in order to measure the anode and cathode potentials individually (Publications II-IV). In the third configuration, rotary screen printed electrodes were manufactured on PET-coated cardboard. Commercial carbon ink, used as a current collector, was printed first on the PET side of the cardboard and enzymatic inks were printed on top of that. The EBFCs were assembled by sandwiching the electrodes on top of each other, separated by membrane, and compressed between planar end-plates. (Publications IV-V).

3.1 Manufacturing methods

3.1.1 Immobilisation and stabilisation of enzymes

When enzymes are purified and removed from their natural environment, they may need to be immobilised and stabilised into structures that can mimic their optimal surroundings. Different immobilisation techniques utilizing polymers have been very successful for this purpose, including physical entrapment and covalent binding [30], [84]. In Publication I, two different modified polymers were used to encapsulate ALDH. Both polymers are micellar, but their chemical microenvironments are very different [85]. The first polymer was Nafion-based and the second chitosan-based. In Publications II and III, commercial carbon-based ink with a low concentration of volatile organic compounds was used to prepare enzymatic inks. This ink was enhanced with multi-walled carbon nanotubes (MWCNT) in order to increase its electron transfer properties (see Appendix A for more details). In Publications IV-V, in-house produced graphite-based inks were prepared and tested using different concentrations of polymers. Polymers tested were polyethylene oxide (PEO), carboxymethyl cellulose (CMC) and medium molecular weight chitosan.

3.1.2 Preparation of enzymatic inks

Catalytic inks are principally made of solvents, binders, conductive components and active components. In this thesis water, water-soluble polymers, carbon, and enzymes and mediators were used, respectively. Rheology and surface chemistry of the ink are fundamental material characteristics that describe ink flow and wetting of the substrate [86]. The rheological behaviour of screen-printable ink should preferably be thixotropic: the ink is thick when resting and becomes thinner when squeezed and pressed through the screen [87]. The adhesion and surface chemistry can be studied via the strength of attraction between the substrate material and the ink - the higher the substrate's surface free energy relative to the ink's surface

tension, the greater is the attraction. As an example, the typical surface free energy of polymers is ca. 30-40 mN cm⁻¹ and the surface tension of water is 72 mN cm⁻¹, rendering water-based inks unsuitable for printing on untreated polymers [88].

Rheology and the surface tension of an ink can be tailored by using different polymers and solvents. Due to the use of enzymes, water was selected as the main solvent of the inks. For this reason, water-soluble polymers had to be used as binders.

In addition to ink characteristics, drying is also a crucial step in R2R manufacturing. Hence, drying of enzymatic inks was studied at different temperatures. Enzymatic activity of the dried electrodes was measured immediately after drying and after 14 and 28 days of storage at room temperature and in a fridge (Publication IV).

Typically, a base ink containing graphite powder and binder polymer (dissolved in water) was prepared. Enzymatic inks were mixed by adding enzyme and mediator into the base ink. Buffer solution was used to adjust the thickness of the ink. Different concentrations of enzyme and mediator were also studied (Publications IV and V).

3.1.3 Printing process of enzymatic electrodes

The aim of this thesis work was to investigate how production of printable enzymatic electrodes can be scaled up from laboratory scale to R2R pilot production. First trials were conducted in the laboratory using rod-coating and a laboratory scale screen printer. The rod-coating technique was used in Publications II and III. Both a laboratory scale screen printer and a pilot scale rotary screen printer were used in Publications IV and V.

Rod-coating was performed using a K Hand Coater (RK Print Coat Instruments Ltd.) with a rod-producing wet layer of 40 μm (Figure 8a). Filter paper (Whatman 1, 180 μm thick) was typically used as the printing substrate. Printed layers were left to dry at room temperature overnight. The electrodes were cut from the substrates for cell assembly (typically 4 cm² or 12.25 cm²).

Laboratory scale screen printing was carried out with a semi-automatic Kent SP-400 screen printer (Figure 8b). The printing screen mesh was NMC EX 31-100 (producing a 70 μm thick wet ink layer), and typically the printing substrate was an insulator paper (Terkab Ilam Delfort Group, 33 μm thick). Enzymatic inks were screen-printed onto an A4-size substrate and dried at room temperature overnight. Each electrode was typically 12.25 cm² and the electrodes were cut from the A4-sheet before assembly.

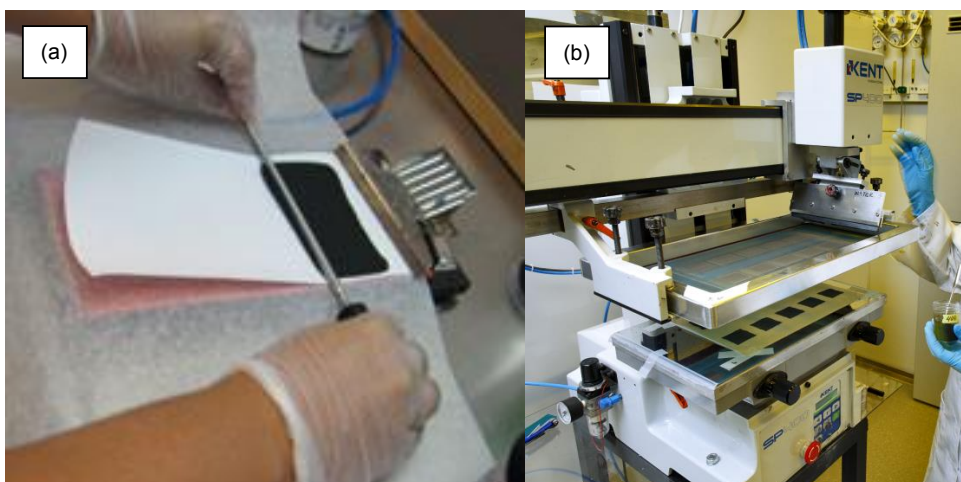


Figure 8. (a) Rod-coating system and (b) Kent SP-400 screen printer used in this thesis work.

Pilot scale rotary screen printing was performed with VTT's modular ROKO printing machine with a printing speed of 2 m min^{-1} (Figure 9a). Gallus BY Mesh 64 (thickness $200 \mu\text{m}$, producing a $100 \mu\text{m}$ thick wet ink layer) printing screens were used for all the inks. A roll of PE-coated cardboard was used as the printing substrate (Figure 9b). Printed layers were dried on the printing line with three 0.9 m long hot air blasting dryers (81 s total drying time). Current collectors (12.25 cm^2) were printed first using a commercial carbon-based ink and dried at $145 \text{ }^\circ\text{C}$. Enzymatic electrodes (9 cm^2) were printed on current collectors in a separate printing run. The anode ink was dried at $72 \text{ }^\circ\text{C}$ and the cathode ink at $65 \text{ }^\circ\text{C}$. Layouts of the printing screens can be found in Supplementary Material 1 in Publication IV.

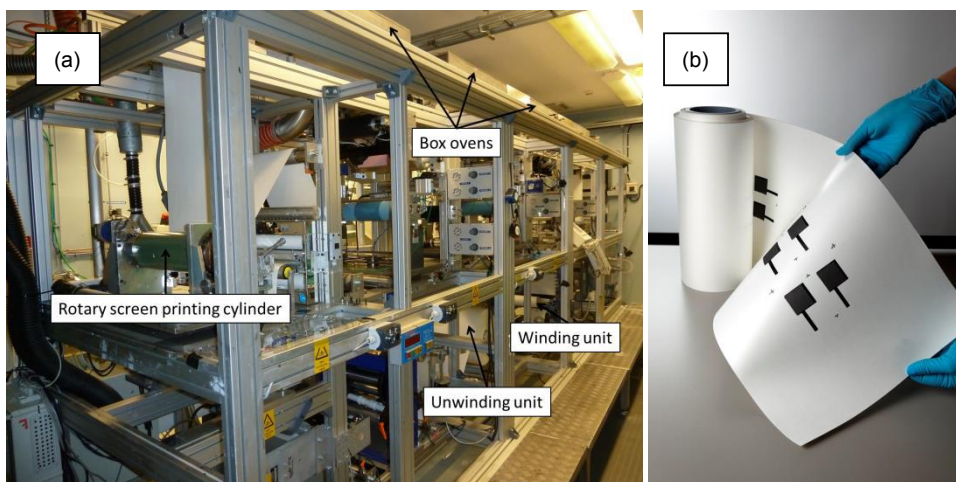


Figure 9. (a) Schematic of VTT's ROKO R2R pilot line and (b) a roll of printed enzymatic electrodes. (Publication IV)

3.2 Morphology of electrodes

Morphology of the electrodes was studied using scanning electron microscopy (SEM) for electrode structure (Publication I), a Dektak stylus profilometer for thickness and a Wyko white light interferometer for roughness (Publications IV and V). Visual determination by means of photography was also used to study adhesion of the printed layer (Publication VI).

3.3 Enzyme activity measurements of printed electrodes

Detection of enzymatic activity of printed electrodes was based on measuring the consumption of dissolved oxygen in the enzymatic reactions, Equations (8) and (14). Dissolved oxygen was measured using a fibre-optic oxygen meter (OXY-10 PreSens). The principle of the meter is based on the quenching of luminescence caused by collision between molecular oxygen and luminescent dye molecules in the excited state [89]. Values for oxygen consumption rate obtained for different electrodes were used for relative comparison, not to determine their absolute quantitative activity. (Publication IV)

3.4 Cell assemblies

3.4.1 Liquid cell

Liquid cell (L-cell) configuration is a modification of the traditional diffusion cell design illustrated in Figure 1a. L-cell (Figure 10) reduces the distance between the cathode and the anode. A platinum gas diffusion electrode is hot-pressed to a Nafion® 112 membrane and clamped between two glass tubes. Thus, the

cathode is in direct contact with air, which eliminates limitations of lack of oxygen. The upper glass tube contains the bioanode and the fuel solution forming a half enzymatic BFC. This cell assembly was used in Publication I, in which immobilised ALDH anodes were characterized.

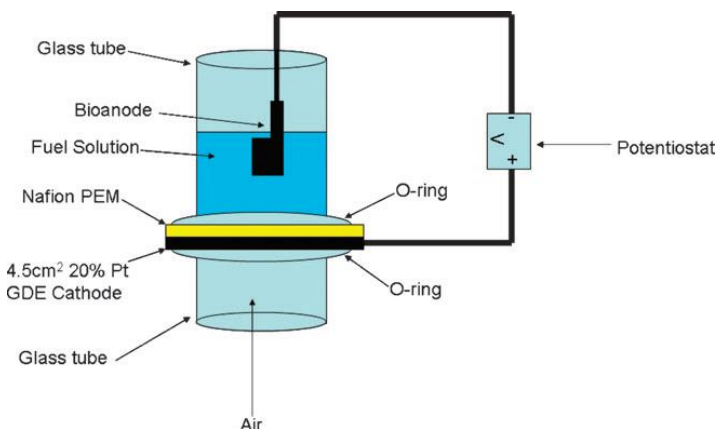


Figure 10. Schematic of the L-cell design used for half enzymatic BFCs with air-breathing platinum cathodes. (Reprinted from [26] with permission.)

3.4.2 Stand-alone cell

Stand-alone cell configuration (Figure 2 in Publication III) was used to characterize EBFCs that were assembled using printed electrodes, both at the anode and cathode. The electrodes (typically 12.25 cm²) were printed on a cellulose-based substrate and sandwiched between graphite end-plates. The printed sides of the electrodes were facing graphite, and no additional membrane was needed between the electrodes. Glucose (50 mg) was spread on the anode before moisturising the cell. The anode end-plate contained holes through which cells were moisturized by pipetting 400 µl of electrolyte into the cells.

3.4.3 Pd/H₂ reference electrode cell

Individual electrode potentials of the anode and cathode half cells were measured using a thin reference electrode inside the separator-membrane. A palladium-hydrogen (Pd/H₂) electrode was chosen due to its inert characteristics especially in acidic electrolyte. Palladium is known to be an excellent hydrogen absorber, able to absorb 900 times its own volume of hydrogen at room temperature. As solid palladium foil is electrochemically charged by hydrogen, these two phases form a constant potential of approximately +50 mV vs. NHE. This potential is independent of the amount of hydrogen absorbed over a wide range. This makes Pd/H₂ an ideal material for a reference electrode, because in hydrogen saturated form it will not disturb the flow of ions in the fuel cell. This reference electrode was adapted from the study by Fleischmann and Hiddeston [90]. Cells were assembled by sandwiching the anode and cathode layers (typically 6.25 cm²) between graphite current collectors and placing a hybrid separator-membrane layer between the anode and cathode. A Pd/H₂ reference electrode was placed inside the hybrid layer (Figure 1 in Publication II). The

anode and cathode layers were moisturised by 200 μ l of buffer-electrolyte (25 mg glucose in 50 mM Na-succinate pH 5).

3.4.4 Cardboard cell

Pilot-manufactured printed enzymatic electrodes were cut from cardboard rolls as illustrated in Figure 11a. First, the anode was moisturised with the glucose-containing buffer electrolyte and the separator was placed on top of the anode. The cathode was then moisturised with the buffer-electrolyte and electrodes were sandwiched between flat plates to ensure even compression pressure (Publications IV and V). In Publication VI, superabsorbent polymers (SAP) were tested as an anode support. In this case the SAP-powder was spread on the anode before moisturizing it. SAP-powder absorbed the anode electrolyte and swelled before the cell assembly, preventing electrolyte from leaking out of the cell (Figure 11b).

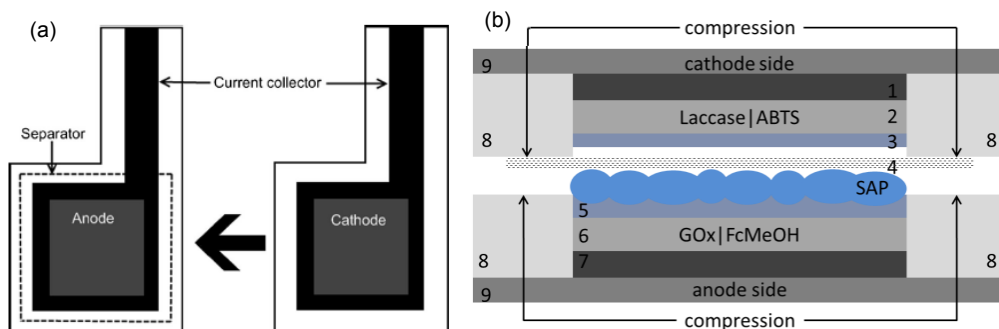


Figure 11. (a) Illustration of the electrode assembly of pilot scale fabricated enzymatic electrodes on cardboard substrate. (Publication IV); (b) Cross-sectional schematic of the cell assembly with SAP on the anode side. The numbers indicate different layers of the cell: 1) printed current collector, 2) printed cathode, 3) cathode electrolyte, 4) membrane, 5) anode electrolyte, 6) printed anode, 7) printed current collector, 8) rubber seal, and 9) printing substrate (cardboard). (Publication VI)

3.5 Electrochemical methods

In order to understand the intermolecular electron transfer between substrates and enzymes, and intramolecular electron transfer between different redox centres within one macromolecule, it is important to measure the redox potentials of enzymes, their co-factors and mediators. The thermodynamic equilibrium potential, E , of an electrode reaction is given by the Nernst equation [91]:

$$E = E^{0'} + \frac{RT}{nF} \ln \left(\frac{c_O}{c_R} \right), \quad (15)$$

where c_O and c_R are the concentrations of the oxidized and reduced species, respectively, and

$E^{0'}$ = formal potential
 R = gas constant
 T = temperature
 n = number of electrons
 F = Faraday constant.

At equilibrium, the cell potential, E_{cell} , is:

$$E_{\text{cell}} = E_c - E_a, \quad (16)$$

where

E_c = potential at the cathode
 E_a = potential at the anode.

3.5.1 Voltammetric measurements

Voltammetry is a very common method for characterizing enzyme-containing electrodes. In cyclic voltammetry (CV), the electrode potential is scanned linearly as a function of time and the resulting current is measured. With CV, the redox potential of the enzyme, cofactor or mediator can be determined. Voltammetry can also show the enzyme's ability to catalyse fuel oxidation or oxygen reduction by either DET or MET. In a reversible redox system, the formal potential can be determined from the voltammogram (Figure 12) and Equation (17):

$$E^{0'} = \frac{E_a^{\text{p}} + E_c^{\text{p}}}{2}, \quad (17)$$

where

E_a^{p} = potential of the oxidation peak (anodic)
 E_c^{p} = potential of the reduction peak (cathodic).

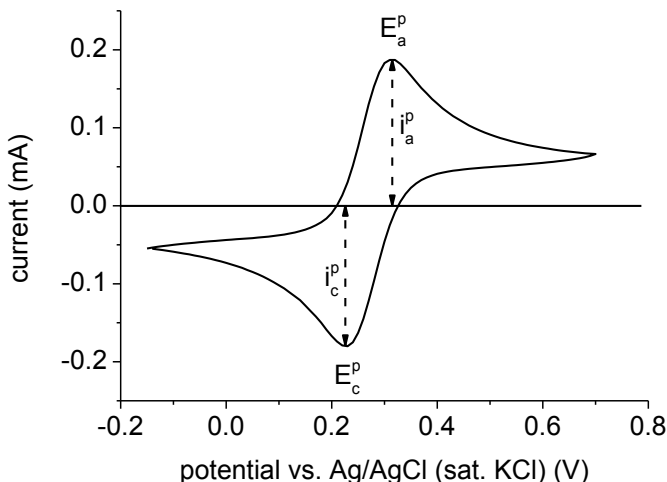


Figure 12. Cyclic voltammogram at 25 mV s^{-1} of an Au-electrode ($r = 2.5 \text{ mm}$) in 1 M KCl with $7.5 \text{ mM Fe(CN)}_6^{3-}/\text{Fe(CN)}_6^{4-}$. The anodic and cathodic peak potentials are indicated as well as the peak currents. The counter electrode was Pt-wire and the reference electrode Ag/AgCl (sat. KCl). (Unpublished)

When scanning the potential at different scan rates, the Randles-Ševčík equation can be used, which at $25 \text{ }^\circ\text{C}$ reduces to [91]:

$$I^p = 268,600 n^{3/2} AD^{1/2} cv^{1/2}, \quad (18)$$

where

- I^p = peak current [A]
- A = area of the electrode [cm^2]
- D = diffusion coefficient [$\text{cm}^2 \text{ s}^{-1}$]
- c = concentration of the analyte [mol cm^{-3}]
- v = scan rate [V s^{-1}].

In practice this means that for a reversible process the peak currents of the redox reactions are linearly dependent on the square root of the scan rate. This theory can be used to study electron transport properties and the active area of different electrode materials (see Appendix A for more details).

3.5.2 Potentiometric measurements

Potentiometry measures the potential between a working electrode and a reference or counter electrode. In the case of enzymatic electrodes, it is an advantage that the enzymes are typically highly selective for a certain analyte, which makes this measurement technique very informative. The potential measured can be

related to the concentration of the analyte of interest. For this reason, potentiometry is one of the most common and simplest evaluation tools to measure the electrochemical potential of a cell at open circuit (OCV). However, this provides information about the thermodynamics but not the kinetics of the cell.

One variant of potentiometry is chronopotentiometry (CP), in which a constant current is applied to the working electrode and the potential of the cell is measured as a function of time. This technique was used to study the operating life of the biobattery (Publications IV-VI). A polarisation curve (iV-curve) can be measured as the current is increased from OCV to a cut-off potential ($E_{\text{cut-off}}$) in steady-state steps. The CP technique was used in Publications II-IV.

3.5.3 Amperometric measurements

Amperometry is a measurement of electric current as a function of time or electrode potential. In chronoamperometry (CA), a constant potential is applied to the cell and the current output of the cell is measured as a function of time. CA measures transient current response under a specific potential until the cell reaches a steady state. Bio-anodes are typically characterised by measuring their calibration curve by CA (Publication I). The potential of the bioanode is maintained constant, ensuring continuous oxidation reaction, and substrate is added to the electrolyte in suitable steps. The current is measured versus substrate concentration, c , and deriving Equation (19) from Equation (6) it is possible to determine maximum biocatalytic current, I_{max} , and Michaelis-Menten constant, K_m .

$$I = \frac{I_{\text{max}}c}{K_m + c} \quad (19)$$

The iV-curve can be measured as the potential is reduced from OCV to a $E_{\text{cut-off}}$ in steady-state potential steps. This technique was used in Publications IV-VI.

3.5.4 Coulometric measurements

In coulometry, constant current or potential is applied to the cell in order to convert the analyte from one oxidation state to another. In this thesis, a constant resistor was used to discharge the biobatteries. Since the total charge is measured, this technique can determine the coulombic efficiency and the energy density of a battery. Electrical charge density (\mathbf{Q}) and electrical energy density (\mathbf{E}) were calculated from the measurement data according to Equations (20) and (21). This technique was used in Publications I-VI.

$$\mathbf{Q} = \int \frac{I}{A} dt = \int \frac{E}{AR} dt \quad (20)$$

$$\mathbf{E} = \int \frac{P}{A} dt = \int \frac{EI}{A} dt = \int \frac{E^2R}{A} dt \quad (21)$$

4. Research contribution

This chapter presents the measurement results and their contribution to the research topics defined in Chapter 1.2. Main results both from published and unpublished research are presented as well as conclusions for the following research. A short discussion on each topic is also presented.

4.1 Immobilized ALDH Bioanodes (Publication I)

In Publication I, ALDH was immobilized on carbon paper using two different polymers. The first polymer tested was tetrabutylammonium bromide (TBAB)-modified Nafion and the second was butanal-modified chitosan. Both polymers are micellar and can be used to immobilise and stabilise different enzymes on carbon electrodes. ALDH anodes were characterized both in three-electrode and L-cell configuration using TMPD as mediator.

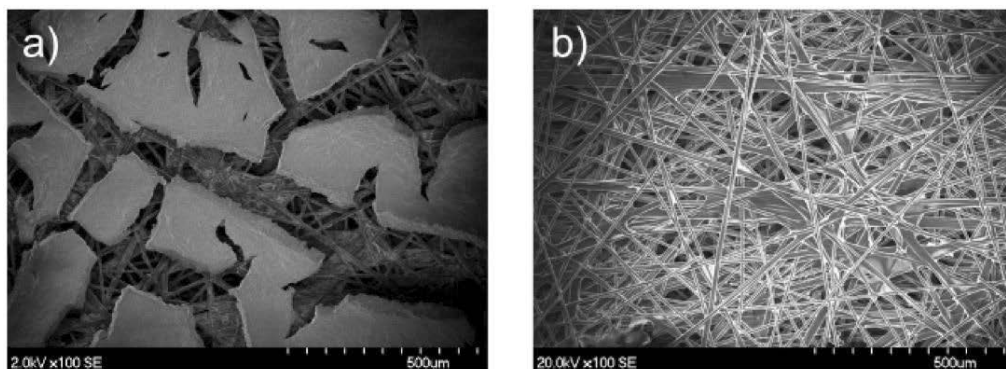


Figure 13. SEM images of (a) TBAB-modified Nafion/ALDH and (b) butanal-modified chitosan/ALDH on Toray paper, 100x magnification. (Publication I)

SEM images (Figure 13) of the electrodes showed that the polymer spread differently on the carbon support: chitosan forms an even layer, whereas Nafion dries forming polymer blocks. The micellar structure of hydrophobically modified chitosan is also larger and less ordered than that of Nafion. These physical properties of enzyme layers were also observed in electrochemical measurements, storage stability and leaching of enzyme. For example, the maximum current density of butanal-modified chitosan bioanodes was fourfold that of TBAB-modified Nafion (Figure 14a), but the storage stability was significantly better with the latter polymer (Figure 14b). The Michaelis-Menten constant (K_m) was the same with both polymers, as was operational stability. Characteristics of the ALDH anodes are presented in Table 1.

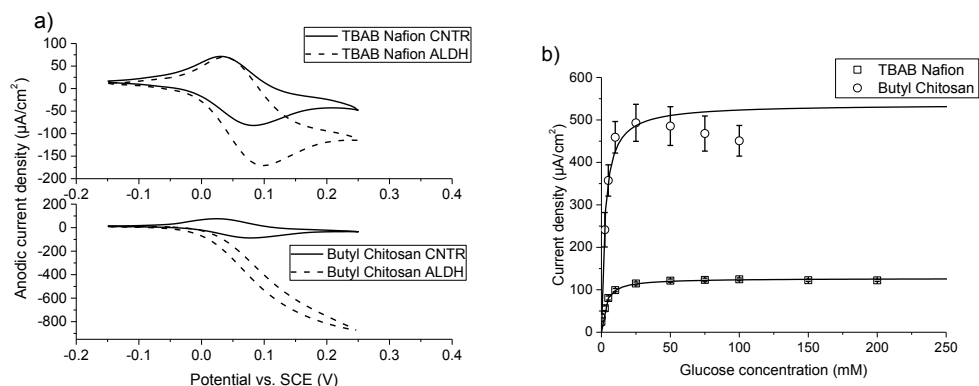


Figure 14. (a) Cyclic voltammogram and (b) calibration curve of immobilized ALDH enzyme on carbon paper. (Publication I)

Table 1. Characteristics of bioanodes and a half enzymatic BFC made of immobilised ALDH.

	Butanal chitosan	TBAB Nafion
K_m	2.6 ± 0.6 mM	2.9 ± 0.6 mM
I_{max}^a	493 ± 44 $\mu\text{A cm}^{-2}$	121 ± 4 $\mu\text{A cm}^{-2}$
I_{max}^b	220 ± 31 $\mu\text{A cm}^{-2}$	112 ± 35 $\mu\text{A cm}^{-2}$
P_{max}^b	15 ± 1 $\mu\text{W cm}^{-2}$	10 ± 4 $\mu\text{W cm}^{-2}$
E_{24h}^b	102 ± 8 $\mu\text{Wh cm}^{-2}$	75 ± 14 $\mu\text{Wh cm}^{-2}$
Leaching _{max}	28%	4%
Stability _{RT,30d}	0%	app. 60%
Stability _{4C,30d}	app. 25%	app. 70%

^a From calibration curve, three electrode setup

^b From L-cell setup, Pt cathode and Nafion 112 membrane

This study showed that ALDH enzyme could be used as an anode enzyme in a fuel cell setup. For this reason, the next study concentrated on testing ALDH in a fully enzymatic fuel cell setup. For mass-manufacturing of enzymatic electrodes, the choice of suitable immobilising polymer had to be considered in terms of performance, price and suitability for screen printing. Due to the biocompatibility and availability of chitosan, it appeared to be a better choice for large scale manufacturing. The only drawback of chitosan was its leaching, because ALDH was stored in buffer, but this was not seen as a problem in the future as the biobatteries were planned to be stored as dry.

4.2 Printed mediated ALDH/ThL EBFCs (Publications II and III)

In Publications II and III, fully printed EBFCs were developed using a rod-coating printing technique. The cells were characterized both in stand-alone and Pd/H₂ reference electrode cell configurations. The former

was used to measure energy density by coulometry and the latter to measure power-curves with CP. The enzyme on the anode was ALDH or GOx and on the cathode ThL or rMaL. Different osmium-based compounds were tested as redox mediators in addition to conventional mediators, i.e. TMPD for anode and ABTS for cathode (Table 2). Overall, the results showed that the best EBFC performance was achieved by using ALDH and ThL as the anode and cathode enzymes, respectively.

Table 2. Redox potential and OCV of individual electrodes using different enzyme-mediator couples. OCV values were measured in a Pd/H₂ cell. They were not published in Publications II and III.

Enzyme	Mediator	Redox potential (mV vs. Ag/AgCl)	OCV _{electrode} (mV vs. NHE)
ThL	ABTS	500, pH 4.5	810 ± 50, pH 5
ThL	[Os(dcbpy) ₂ (4-AMP)Cl]PF ₆	445, pH 4.5	670 ± 50, pH 5
rMaL	ABTS	500, pH 7	700, pH 6.5
ALDH	TMPD	70, pH 7	260 ± 60, pH 5
ALDH	Os(bpy) ₂ Cl ₂	0, pH 7	180 ± 20, pH 5
GOx	TMPD	70, pH 7	400, pH 5
GOx	Os(bpy) ₂ Cl ₂	0, pH 7	400, pH 5

Unpublished Pd/H₂ cell measurements (Figure 15 and Figure 16) showed that although solution phase studies indicated a redox potential of 700 mV vs. NHE for the ThL/ABTS couple, the OCV of ThL/ABTS cathode was 810 mV in the case of a full EBFC. This potential is higher than would have been expected. Additionally, GOx electrodes showed higher OCV than expected, which can be attributed to the fact that at pH 7 and pH 5 the reduction of O₂ to H₂O₂ occurs at 0.29 V and 0.4 V vs. NHE, respectively. Thus decreasing the anode pH increases the potential in the case of GOx. Other enzyme-mediator couples showed predictable OCV potentials (Table 2). The same behaviour was also seen in the OCV of EBFCs (Table 3): the highest OCV was 620 mV, although solution phase studies predicted only 500 mV.

The reason for higher ThL/ABTS potential in a fuel cell setup should be discussed. Laccase-mediator systems (LMS) have previously been shown to oxidise aromatic alcohols and hydrocarbons even though the oxidation potential was higher than the redox potential of the LMS [92]–[94]. ABTS undergoes two one-electron redox reactions at ca. 680 and 1090 mV vs. NHE at pH 4-5 [92], [93], [95], which correspond to the oxidation/reduction of ABTS/ABTS^{•+} and ABTS^{•+}/ABTS²⁺, respectively. The stabilities of these redox states are dependent on solution composition, pH and electrode material. Although high potential laccases have their T1 Cu site redox potential at ca. 790 mV vs. NHE, which is almost 300 mV lower than the oxidation reaction of ABTS^{•+}/ABTS²⁺, the oxidation reaction is possible at a very slow rate. By using the Nernst equation (15), and redox potentials of ABTS^{•+}/ABTS²⁺ and ThL T1 Cu, it is possible to calculate the equilibrium constant $K = c_{O}^0/c_{R} = 5.32 \cdot 10^{-6}$. This reaction is thermodynamically unfavourable but possible if the reac-

tion is driven forward by a follow-up process that irreversibly removes one of the products from the equilibrium of the first reaction [92], [93]. As an example, results reported by Bourbonnais et al. [92] showed that bulk electrolysis of ABTS and veratryl alcohol ($E_{p,a} = 1175$ mV) at 585 mV (vs. Ag/AgCl) resulted in the formation of verataldehyde, thus showing that ABTS can be oxidised to $ABTS^{2+}$ at significantly lower potential than expected. In addition, Dong et al. [96] reported that addition of graphene into a laccase-ABTS system increased the removal of labetalol, which was attributed to the formation and release of $ABTS^{2+}$.

Hence, this data suggests that in the case of ThL/ABTS couple incorporated into MWCNT-modified carbon ink, both redox reactions of ABTS can take place. This is possible because ThL is a high potential laccase with a redox potential of the T1 Cu site ca. 780 mV at pH 6.5 and ca. 840 mV at pH 5 (see Appendix B), which is sufficient to slowly oxidize $ABTS^+$ to $ABTS^{2+}$. This was also visually seen as the biofuel cells were opened after use: both blue-green ($ABTS^+$) and purple ($ABTS^{2+}$) colours were noticed. As both cations were present on the cathode side, and being separated with a semipermeable membrane from the anode, an unpredictable high cathode potential was created.

Table 3. OCV, maximum power density and energy density of different cathode-anode pairs. OCV values were not published in Publications II and III.

Cathode	Anode	OCV (mV)	P_{max} ($\mu W cm^{-2}$)	E as $V > 200$ mV ($\mu Wh cm^{-2}$)	Duration of the measurement (h)
ThL/ABTS	ALDH/ Os(bpy) ₂ Cl ₂	620 ± 10	3.50	11.1 ± 5.5	47
ThL/ABTS	ALDH/TMPD	560 ± 10	1.67	10.7 ± 2.8	74
ThL/ [Os(dcbpy) ₂ (4-AMP)Cl]PF ₆	ALDH/ Os(bpy) ₂ Cl ₂	490 ± 10	0.39	16.3 ± 2.2	123
ThL/ [Os(dcbpy) ₂ (4-AMP)Cl]PF ₆	ALDH/TMPD	430 ± 10	0.30	4.4 ± 0.1	58
rMaL/ABTS	ALDH/ Os(bpy) ₂ Cl ₂	520	0.50	15	98
rMaL/ABTS	ALDH/TMPD	470	0.39	9	78
ThL/ABTS	GOx/TMPD	370	0.28	0.12	2.0
ThL/ABTS	GOx/ Os(bpy) ₂ Cl ₂	360	0.17	0.02	0.8

The maximum power density was measured using CP with addition of 0.2 μA every minute (referred to as fast scan). In order to obtain high power from the cell, both the potential and current density need to be maximized. Therefore, the cells with highest OCV can be predicted to give the best performance provided that the rate of electron transfer between enzyme-mediator and mediator-electrode is sufficient. Fast scan iV-curves (Figure 15 and Figure 16) showed that ThL worked significantly better than rMaL. ThL also per-

formed better with ABTS than [Os(dcbpy)₂(4-AMP)Cl]PF₆. ALDH/TMPD was unstable at higher current densities than ALDH/Os(bpy)₂Cl₂ and GOx electrodes were very unstable and did not perform well. The highest power density was achieved with ALDH/Os(bpy)₂Cl₂ anode and ThL/ABTS cathode.

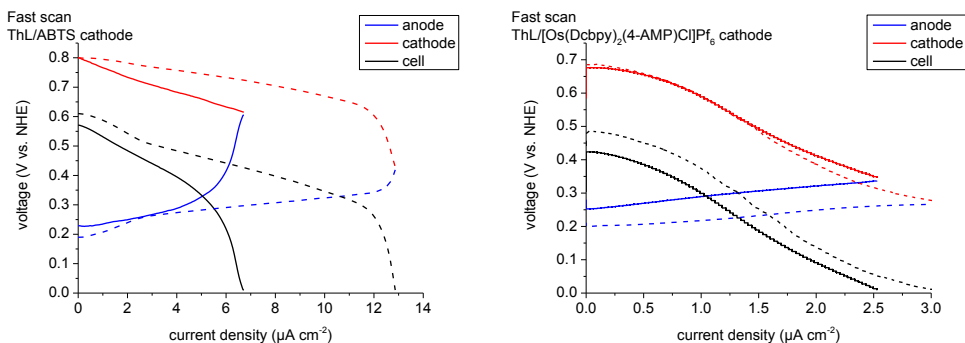


Figure 15. iV-curves of EBFCs with ALDH anode using TMPD (solid) or Os(bpy)₂Cl₂ (dashed) as mediator. The cathode was ThL/ABTS (left) or ThL/[Os(dcbpy)₂(4-AMP)Cl]PF₆ (right). Geometrical cell area 6.25 cm². Fast scan was measured using CP in 0.2 µA intervals every minute. (Unpublished)

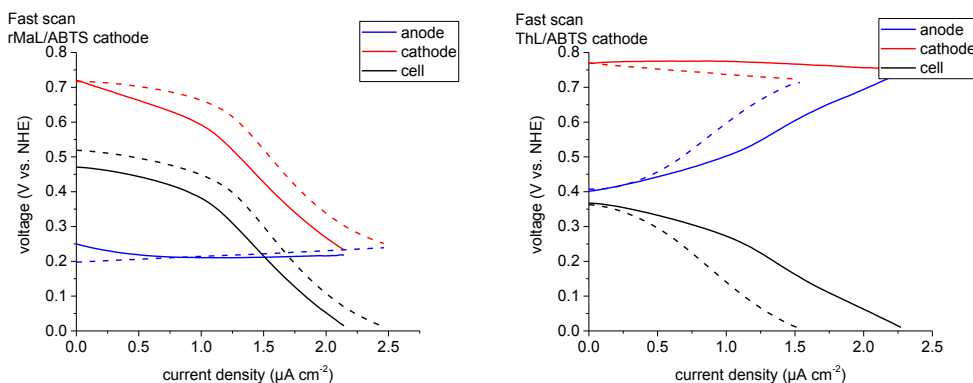


Figure 16. iV-curves (left) of ALDH/rMaL EBFCs with TMPD (solid) or Os(bpy)₂Cl₂ (dashed) as anode mediators. iV-curves (right) of GOx/ThL EBFCs with TMPD (solid) or Os(bpy)₂Cl₂ (dashed) as anode mediators. The cathode mediator was ABTS in all cases. (Unpublished)

Surprisingly, stand-alone cell measurements (referred to as slow scans) showed that the ALDH/ThL cell with osmium-mediators both on the anode and cathode was the most stable. The second best slow scan performance was achieved with ALDH-anode and rMaL-cathode. Overall, this data showed that fast scan measures the maximum catalytic performance of different enzyme-mediator pairs, whereas slow scan indicates the long-term stability of enzyme-mediator pairs. For this reason, it is important to pay attention to the

measurement techniques used in order to study the appropriate characteristics, in this case maximum power output vs. maximum energy output.

4.3 Scale-up of manufacturing (Publication IV)

In Publication IV, the manufacturing process of enzymatic electrodes was scaled up from laboratory to pilot scale. The idea was to select materials which were as commercially applicable as possible. For this reason, some materials were chosen based on their availability, price and safety over their performance.

The first task was to modify in-house made inks for screen printing. Due to the use of enzymes, a water-based buffer solution was chosen as the medium of the ink. The selection of the binder was made between CMC and PEO due to their water solubility and safety. Graphite was selected as the conductive component of the ink. Carbon nanotubes were rejected due to their difficult handling properties in large quantities and relatively high price. Due to its availability, price and stability, GOx was preferred as the anode enzyme rather than ALDH. Three different ferrocene-based redox molecules were tested as anode mediators for GOx with regard to their safety. TMPD was rejected due to its poor performance with GOx, as observed in Publications II and III. Ferrocenemethanol (FcMeOH) showed the highest catalytic current at the lowest potential (half wave potential around 250 mV vs. Ag/AgCl). Laccase/ABTS was chosen as the cathode enzyme-mediator pair due to its good functionality and stability, even though ABTS is relatively expensive.

Performance properties of the laboratory scale screen printed electrodes were characterized with CP measurements (Figure 17a). It was clear that PEO functioned better as the binder in GOx/ThL cells. Both enzyme activity (oxygen consumption) of laccase and Pd/H₂ cell measurements showed that the laccase cathode was inactivated when CMC was used as the binder. This was most probably due to the anionic nature of CMC, which acts as a resin, trapping positively charged ThL into the structure and thereby deactivating the enzyme.

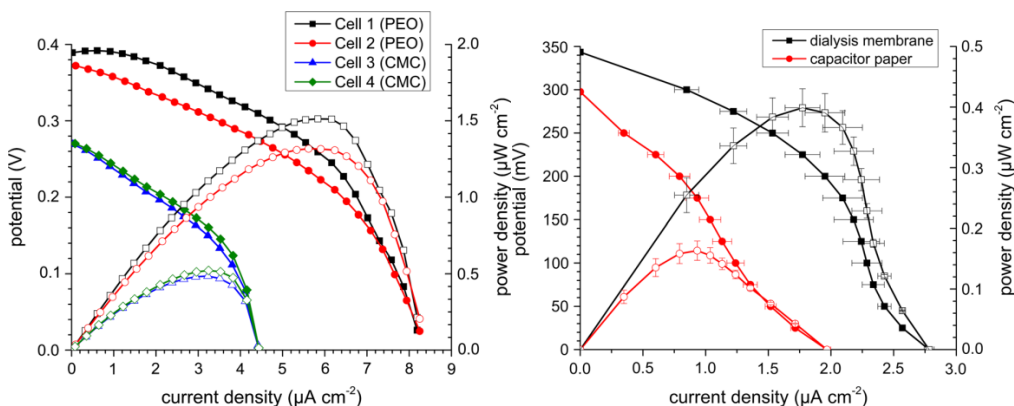


Figure 17. iV and power curves of EBFCs manufactured using a laboratory scale screen printer (left) and a pilot scale rotary screen printer (right). Two different binders and separators were tested for ink preparation and cell assembly. (Publication IV)

Drying experiments (1 min at elevated temperature) with enzymatic inks showed that enzymes alone can withstand relatively high temperatures; even a temperature of 90 °C reduced the enzymatic activity only by 20-30% (Figure 18). After 28 days of storage at room temperature, the residual activity was still 50-60% of the original. However, when the mediators were mixed into the enzymatic inks, the activity of the electrodes decreased dramatically during storage. After 28 days, the activity was only around 20-30% of the initial level. This indicates that mixing mediators with the enzymes in the ink may not be the best strategy in terms of stability.

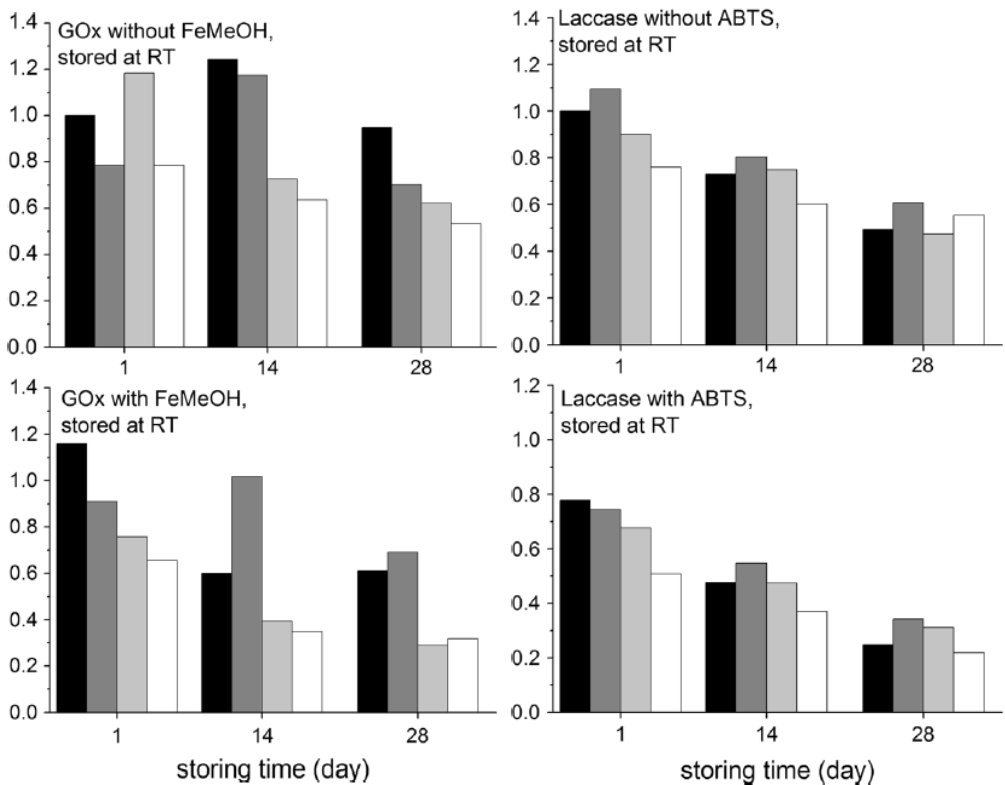


Figure 18. Relative enzyme activity (oxygen consumption) of GOx and EcoL electrodes dried at different temperatures and stored at room temperature. Drying temperatures were 23 °C (black), 50 °C (dark grey), 70 °C (light grey) and 90 °C (white). (Publication IV)

For pilot scale manufacturing, the ink needed to be modified in order to have good print quality in rotary screen printing. Therefore, the base ink contained a higher amount of graphite and a lower amount of binder solution. The base ink was diluted in situ with buffer during the printing trial. The amounts of mediators were also decreased due to their limited availability for large ink batches. First the mediator amount was 40% of

that used in laboratory inks, and in order to compensate for this reduction, a higher amount (2.5-fold) of enzyme was added to the inks. In the pilot printing trial, the inks had to be diluted further with buffer solution in order to adjust the viscosity of the ink. In the end, the composition of the pilot printing inks was drastically different from that of the inks prepared for the laboratory screen printer (Table 4). The amounts of enzyme and mediator per electrode were approximately 190% and 30%, respectively, of those in the laboratory inks. This difference was reflected in the electrochemical performance of the EBFCs assembled using pilot-manufactured electrodes (Figure 17b). The maximum performance (P_{\max} and I_{\max}) of pilot-manufactured cells was approximately 70% lower than those of the laboratory manufactured cells; the energy output was as much as 90% lower. This can be attributed to the lower amount of mediator as well as to the degradation of enzyme-mediator electrodes due to heating (ca. 70 °C) and storage (ca. one week).

Table 4. Composition of inks used in laboratory screen printing and pilot scale rotary screen printing, and electrochemical performance of EBFCs assembled using these enzymatic electrodes.

	Laboratory scale manufacturing (GOx/ThL)	Pilot scale manufacturing (GOx/EcoL)
Graphite amount in wet ink (wt.%)	37	46
Binder amount in the ink (wt.% g ⁻¹ _{graphite})	7	3.6
Enzyme amount in the ink (nkat g ⁻¹ _{graphite})	1000	1544
Mediator amount in the ink (μmol nkat ⁻¹)	0.06	0.01
OCV (mV)	380 ± 8	345 ± 5
P_{\max} (μW cm ⁻²)	1.4 ± 0.1	0.4 ± 0.03
I_{\max} (μA cm ⁻²)	8.35 ± 0.04	2.78 ± 0.04
E as $V > 200$ mV (μWh cm ⁻²)	5.5 ± 0.2	0.6 ± 0.1

4.4 Increasing the performance of the GOx/FcMeOH anode (Publication V)

In Publication V, the long-term stability of the pilot-manufactured electrodes was studied. Based on the laboratory experiments, the anode mediator appeared to be ageing during storage. As a consequence, a new batch of anode ink was developed and the amount of the anode mediator was increased. In addition, in order to increase the physical stability of the enzymatic anode layer, the ink composition was altered by adding more binder (both PEO and chitosan) into the ink. Finding the optimum amount of PEO, chitosan and FcMeOH in the ink was not straightforward, because they all appeared to affect the cell performance. How-

ever, after several laboratory ink experiments the final ink for manufacturing of the second pilot anode contained almost twice the amount of the binder and the mediator. On the other hand, the amount of graphite in the wet ink was 20% lower than in the first pilot ink, which meant a lower amount of enzyme per electrode (Table 5).

Table 5. Composition of the second pilot anode ink. The values in square brackets represent characteristics of the first pilot anode ink.

	2 nd Pilot scale manufacturing (GOx/FcMeOH)
Graphite amount in wet ink (wt.%)	37 [46]
Binder amount in the ink (wt% g ⁻¹ _{graphite})	7.1 [3.6]
Enzyme amount in the ink (nkat g ⁻¹ _{graphite})	1622 [1544]
Mediator amount in the ink (μmol nkat ⁻¹)	0.02 [0.01]
OCV (mV)	341 ± 1 [345 ± 5]
P_{max} (μW cm ⁻²)	0.59 ± 0.02 [0.4 ± 0.03]
I_{max} (μA cm ⁻²)	4.4 ± 0.1 [2.78 ± 0.04]
E as $V > 200$ mV (μWh cm ⁻²)	0.88 ± 0.01 [0.6 ± 0.1]

The second pilot ink enhanced the electrochemical performance of the cells significantly, even though the amount of enzyme per electrode was lower. The improvement was due to the increase in the mediator amount (1.7-fold). However, neither this increase nor adding chitosan into the ink stabilized the anodes - they degraded at same rate as before. On the other hand, physical rigidity did increase, seen as an increased reducibility and an even ink layer.

4.5 SAPs as anode support (Publication VI)

In Publication VI, the operational lifetime of the pilot-manufactured enzymatic biobatteries was extended by adding a super-absorbent polymer (SAP) to the anode side. Addition of SAPs did not significantly increase the maximum power density or the current density. Improved operational stability was most probably due to better contact between anode-membrane-cathode interfaces, which was seen as lowering of IR drops by 14%, and better moisture management in the cell. Images (Figure 1 in Publication VI) also showed that the addition of SAPs prevented delamination of the enzymatic cathode layer from the current collector layer. Water transport through the membrane from the anode to the cathode and moisture retention of the cells were also increased. As an outcome, both electric charge density and energy density were doubled when SAPs were added to the anode (Table 6).

Table 6. Cell characteristics without and with addition of SAP on the anode. Charge and energy density values were calculated using $E_{\text{cut-off}} = 200$ mV.

	no SAP	SAP 1	SAP 2
OCV (mV)	347 ± 4	367 ± 4	366 ± 3
I_{max} ($\mu\text{A cm}^{-2}$)	4.4 ± 0.1	4.2 ± 0.1	4.0 ± 0.1
P_{max}	0.59 ± 0.01	0.58 ± 0.01	0.63 ± 0.01
Q ($\mu\text{Ah cm}^{-2}$)	4.52 ± 0.05	7.1 ± 0.2	9.9 ± 0.4
E ($\mu\text{Wh cm}^{-2}$)	1.14 ± 0.02	1.87 ± 0.01	2.63 ± 0.05

4.6 Further improvements of enzymatic inks

4.6.1 Increase of anode performance by increasing GOx/FcMeOH in the ink and changing the substrate to carbon fibre paper

The possibility to increase the performance of EBFC by increasing the amounts of biocatalyst-components in the anode ink and printing them on a porous carbon fibre felt (Kevra, 20 g m⁻²) was studied. The base ink was DuPont modified with MWCNTs (as in Publications II and III). The original amount of GOx and FcMeOH in the ink used in samples 1-5 was 400 nkat ml⁻¹_{ink} and 0.125 $\mu\text{mol nkat}^{-1}$, respectively (Table 7). A threefold amount of GOx and FcMeOH was used in samples 6-10. The cathode ink contained 400 nkat ml⁻¹_{ink} and 0.125 $\mu\text{mol nkat}^{-1}$ of ThL and ABTS in the ink, respectively, and it was used in all samples.

The inks were rod-coated on the carbon felt. Electrodes (4 cm²) were cut from the substrate before assembly. In cells 1-2 and 6-8 one anode print was used. In cells 3-5 and 9-10 three anode prints were used on top of each other. The layers were assembled between graphite current collectors and separated by a dialysis membrane. The cells were activated by adding 200 μl of buffer electrolyte (25 mg glucose in 50 mM Na-succinate pH 4.5).

Electrochemical characterisation was performed with CP. OCV was measured for two hours (Figure 19a), after which constant current was applied to the cell, increasing the current by 0.1 μA every 20 min (Figure 19b). Each measurement was terminated when the cell potential reached 200 mV.

Table 7. Different cells. E1 represents carbon fibre electrodes containing a 1-fold amount of enzyme and mediator, whereas E3 represents electrodes containing a 3-fold amount of enzyme and mediator. Values are means ± standard deviation. (Unpublished)

Cells	Anode	OCV (mV)	Q ($\mu\text{Ah cm}^{-2}$)	E ($\mu\text{Wh cm}^{-2}$)
1-2	1 x E1	350 ± 30	5 ± 4	1 ± 1
3-5	3 x E1	410 ± 40	29 ± 3	7 ± 1
6-8	1 x E3	380 ± 60	21 ± 5	6 ± 1
9-10	3 x E3	470 ± 10	60 ± 20	19 ± 9

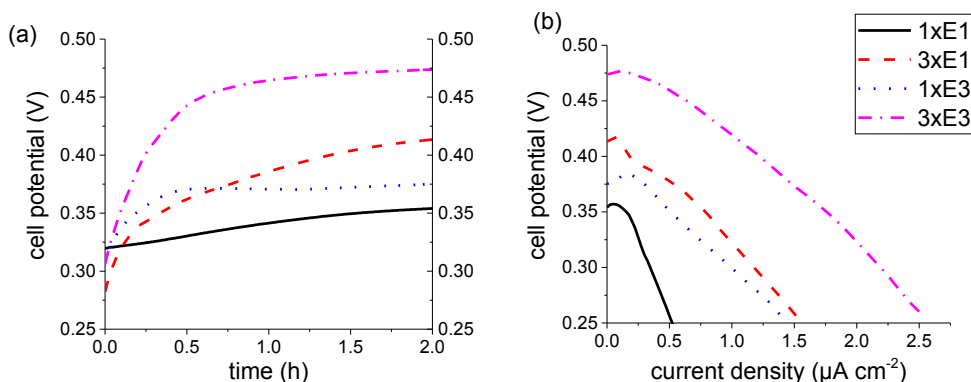


Figure 19. (a) OCV of EBFCs using different amounts of FcMeOH/GOx in the ink and either one or three printed layers on top of each other. (b) CP measurement of the cells. The curves represent average values. (Unpublished)

These preliminary results showed that the GOx-anode could be tailored by adding more catalytic components into the inks and printing them on carbon felt, as well as by stacking electrode materials. The more catalytic components in the ink, the higher were the OCV (most probably due to an increased amount of reduced form of FcMeOH on the electrode surface), charge and energy output. This data suggested that multilayer printing could also be a means to increase the cell performance.

4.6.2 Changing graphite to carbon black in enzymatic inks

The possibility to substitute carbon black (CB, Printex XE2) for graphite in enzymatic inks was studied. Figure 20 shows SEM images of both carbons used; CB is a very fine powder, whereas graphite is coarser.

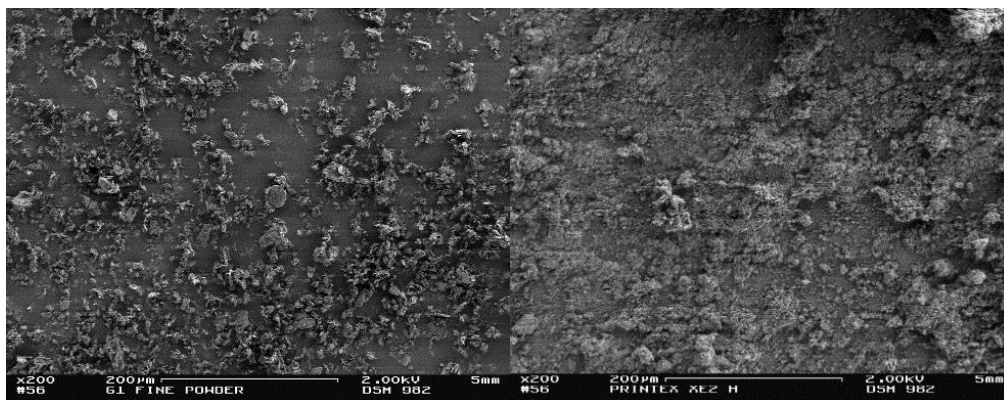


Figure 20. SEM of dry graphite (left) and carbon black (right) powders. Magnification x200. (Unpublished)

Inks without active components were characterised with the ferro/ferricyanide redox couple as described in Appendix A. Both inks contained carbon, PEO (7 wt.% $\text{g}^{-1}_{\text{carbon}}$) and buffer (Table 8). The amounts of graphite and CB in the inks were 39 wt.% and 8.7 wt.%, respectively. Cyclic voltammograms showed that the redox peaks of the graphite ink were lower compared with those of the CB ink (Figure 21). In addition, CB ink showed capacitive behaviour as its CV curves were rectangular shaped. This can be attributed to the different surface areas of the carbons: ca. $10\text{-}100\text{ m}^2\text{ g}^{-1}$ for synthetic graphites and $1000\text{ m}^2\text{ g}^{-1}$ for Printex XE2. This indicates that these two carbon powders may exhibit different properties in enzymatic inks.

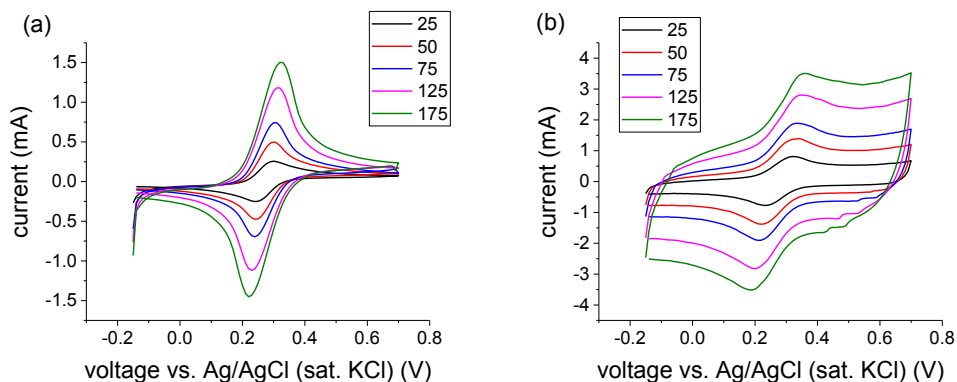


Figure 21. Voltammograms of $\text{F}_3\text{Fe}(\text{CN})_6/\text{F}_4\text{Fe}(\text{CN})_6$ on glassy carbon electrodes coated with (a) graphite ink and (b) CB ink. (Unpublished)

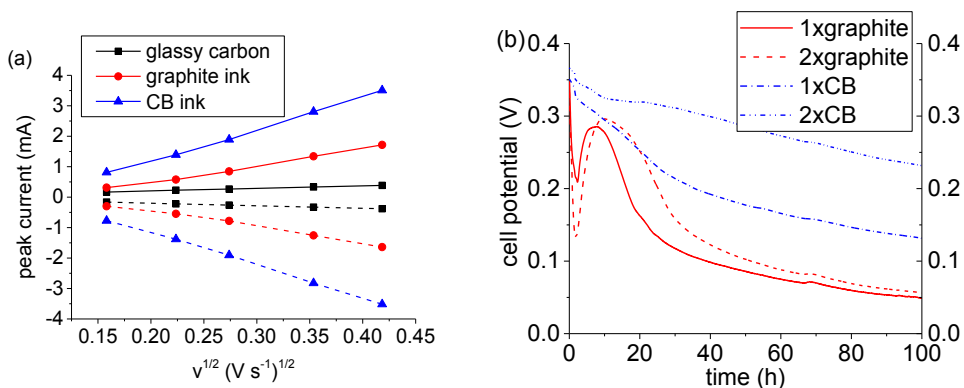


Figure 22. (a) Randles-Ševčík plot of different carbon-based inks on a GC electrode. The electrolyte was 1 M KCl with 7.5 mM of $\text{F}_3\text{Fe}(\text{CN})_6/\text{F}_4\text{Fe}(\text{CN})_6$. Pt-wire was used as counter electrode and Ag/AgCl (sat. KCl) as reference electrode. (b) Discharge-curve (constant load of $75\text{ k}\Omega$) of GOx||ThL cells using two different carbon-based inks. The cell area was 12.25 cm^2 and 50 mg of glucose in $400\text{ }\mu\text{l}$ of 50 mM Na-succinate buffer (pH 4.5) was used to moisturise the cells. 1x indicates one layer and 2x two layers of anode ink. (Unpublished)

The Randles-Ševčík plot also showed significantly different slopes (Figure 22a). The increase in the slopes of the Randles-Ševčík plot is attributed to an increased electrode area, A , in Equation (18). Slopes for the graphite ink and CB ink were 4.9×10^{-3} and 1.1×10^{-2} , respectively. According to these experiments, the active area of the CB ink is 2.2 times greater than that of the graphite ink. As each electrode contained 4 μ l of ink, there was ca. 1.56 mg of graphite and 0.348 mg of CB per electrode. Considering the surface areas of these carbons, a 2.2x increase is reasonable.

When enzymatic inks were prepared from these two carbon materials, different ink compositions were necessary to make them printable (Table 8). The amount of GOx and FcMeOH was the same in both inks, but the dry amount of carbon was significantly different. This had to be taken into account when the cells were compared. In practice, each wet anode (12.25 cm²) print was weighed and the amount of enzyme per print was calculated according to the weight and ink composition. The printing was done directly on graphite current collectors using a printing screen (mesh NMC EX 31-100). Tests were made of both one-layer and two-layer printing.

Table 8. Compositions of the anode graphite ink and the CB ink. (Unpublished)

	graphite ink	CB ink
carbon	2.5 g (39 wt.%)	0.375 g (8.7 wt.%)
PEO (5 wt.% in H ₂ O)	3.5 ml	0.525 ml
buffer (50 mM Na-succinate pH 4.5)	0.4 ml	3.4 ml
GOx (1400 nkat)	560 nkat g ⁻¹ _{carbon}	3730 nkat g ⁻¹ _{carbon}
FcMeOH (19 mg)	0.06 μ mol nkat ⁻¹	0.06 μ mol nkat ⁻¹

The difference in the active area of the inks can be seen in the discharge curves (Figure 22b), as the CB ink performs significantly better than the graphite ink. In fact, the energy outputs of the cells with similar amounts of GOx/FcMeOH were twofold (Table 9). The OCV was also stable and high when the CB ink was used. This indicates that the type of carbon support, especially its active area, in enzymatic inks plays a very important role. Electrochemical properties of home-made carbon inks provide useful preliminary data for planning of the actual enzyme-containing inks. By using a high surface area carbon support it is possible to create a printed BFC/supercapacitor hybrid that is self-charged.

Table 9. Characteristics of test cells. The rows emphasised in light grey denote comparable cells in terms of active component amount. Values are means \pm standard deviation ($n = 3$). (Unpublished)

Anode layer	OCV at 1.5 h (mV)	Weight of wet anode (g)	Calculated enzyme activity per anode (nkat)	E (μ Wh cm ⁻²)
1xgraphite	220 \pm 40 *	0.15 \pm 0.01	33	1.10 \pm 0.04
2xgraphite	140 \pm 70 *	0.31 \pm 0.06	77	1.8 \pm 0.4
1xCB	340 \pm 10	0.24 \pm 0.09	78	3.9 \pm 0.7
2xCB	362 \pm 1	0.35 \pm 0.09	114	12 \pm 5

* unstable

5. Discussion

5.1 Performance

Several factors contribute to the performance of printed biobatteries. First of all, the selection of enzyme-mediator pairs is crucial. In the case of the cathode, high potential laccase (ThL) is preferred due to its capability to reduce oxygen to water close to the theoretical potential. In order to guarantee sufficient electron transfer into laccase, several mediators were tested, of which ABTS appeared to be the most suitable. ThL was able to oxidise both redox states of ABTS; the highest cathode potential was ca. 800 mV vs. NHE (Publications II and III).

Selection of the anode enzyme-mediator pair was made between GOx and ALDH (Publications II and III). The highest performance was achieved using ALDH with an osmium-mediator. The lowest anode potential was ca. 200 mV vs. NHE. The second-best performance was achieved with TMPD, showing an OCV of ca. 300 mV vs. NHE. However, due to the limited availability of ALDH, GOx was preferred as the enzyme. Neither osmium complexes nor TMPD performed well in printed GOx electrodes. The mediator for GOx was selected from the group of ferrocene derivatives, from which FcMeOH showed the best catalytic current at the lowest potential of ca. 450 mV vs. NHE (Publication IV).

After the enzyme-mediator selection, the next step was to understand how the composition of enzymatic inks affects the cell performance. Components in the simplest inks are carbon powder, a binder, an enzyme, a mediator and solvent (aqueous buffer). The type of carbon powder plays an important role because the redox chemistry of mediators takes place on the powder surface. Therefore, the carbon support should have as high an active area as possible. In order to increase its active area, commercial carbon-based ink was modified with MWCNTs. Changing graphite powder to carbon black in the experimental inks improved the cell performance by doubling the 2D active area of the printed layers.

The type of binder must also be taken into account, because some water-soluble polymers may have ionic characteristics that affect the catalytic performance of enzymes. Comparing PEO and CMC showed that the cathode enzyme was not active when CMC was used, most probably due to the anionic property of CMC (Publication IV), and PEO was consequently selected as the preferred binder. The amount of binder is also an important factor for the cell performance. Too low an amount of binder makes the printed layer very fragile, and good conductivity is lost as well as good adhesion to the printing substrate (Publication IV and VI). On the other hand, too high an amount of binder increases concentration overpotentials, and free movement of mediators to the enzymes can be lost (Publication I).

Determining the optimum amounts of active components in the inks was rather complex, as it appears that the type and amount of carbon and the binder affect the optimum amount of enzyme and mediator. However, there were two findings that had good correlation. First, the amount of the mediator is one of the key factors in maximum performance. This is of course obvious, because the mediator carries the charge between the electrode and the enzyme. However, its amount cannot be arbitrarily increased. Second, the amount of available active enzymes as well as the active electrode area are related to the appropriate mediator amount. For example, with graphite, the maximum amount of FcMeOH in the ink is approximately 14 mg g⁻¹_{graphite} (65 μmol g⁻¹_{graphite}). In order to function properly, the anode must have enough active enzyme available. In graphite ink with 7 wt.% of binder, an appropriate amount of GOx was ca. 1000 nkat g⁻¹_{graphite}. If the binder amount was only half of that, a twofold amount of GOx was needed. When a carbon support with a large active area was used, the amounts of active components could be increased, which led to an increase in the energy output. The maximum amounts of active components in the CB ink was not studied

in detail; this would be an interesting topic for further studies. The cell performance could also be increased by stacking anodes on top of each other or by multilayer printing.

Integration of biobatteries with electronics can also improve their performance. For example, with a combination of a stack of printed biobatteries and printed super-capacitors, 5 mA pulses (lasting 3 s) every 20 min could be generated (see Appendix C). This could extend the range of applications from μW scale to mW scale.

5.2 Stability

The stability of printed electrodes can be discussed from three points of view: stability during manufacturing, during storage, and during use. The first enzymatic electrodes were manufactured using the very sensitive ALDH enzyme, immobilised with Nafion or chitosan-based polymers. It was found that the Nafion-based polymer resulted in more stable electrodes in terms of storage stability, but most of the enzymatic activity (in this case available enzyme) was lost due to poor spreading onto the carbon paper. The chitosan-based polymer resulted in a more evenly coated surface on the carbon paper and hence in better electrochemical performance. As a consequence, alternatives to Nafion were searched for.

Since the enzyme electrodes are manufactured using water-based inks at room temperature, there is no dramatic decay in their activity. Especially if there is a long delay (> 1 h) between ink preparation and printing, selection of the solvent becomes important. In order to keep the inks stable, suitable binders and buffers should be used. As the electrodes are dried at elevated temperatures, their enzymatic activity typically decreases. The addition of mediators into the inks decreases the enzymatic activity further in the drying step, most probably due to accelerated thermal degradation as predicted by the Arrhenius equation (not shown).

During one month of storage, printed GOx electrodes lost a maximum of 20-30% of their enzymatic activity, whereas laccase lost 40%, regardless of the drying or storage temperature. However, when mediators were added into the inks, elevated drying temperatures accelerated the degradation, and 70-80% of the enzymatic activity was lost in 28 days. Drying at 50 °C was an exception, perhaps due to PEO's characteristics of having a crystalline melting temperature of 65 °C and being possible to crystallise at 50 °C [97]. It seems that especially GOx/FcMeOH anodes dried at 50 °C benefitted from this property, losing only 20-30% of their enzymatic activity in 28 days, regardless of whether they were stored at room temperature or in a fridge. For laccase/ABTS electrodes, storing in a fridge is most beneficial, as the electrodes lost only 40% of their enzymatic activity. Laccase/ABTS electrodes stored at room temperature degraded faster, ca. 60-70% of the activity being lost in 28 days. This may be due to the fact that storage conditions were neither air- nor moisture-free, and the reaction between laccase and ABTS could continue during storage, thus ageing the laccase electrodes.

Pilot-manufactured electrodes were also characterised electrochemically. Degradation of electrodes was also observed in these measurements. The anodes were found to be the limiting factor for cell performance. Especially the anode mediator degraded, but adding fresh mediator into the activation electrolyte restored the anode performance. Thus, not only the stabilisation of enzymes but also that of mediators is important. There are at least three degradation mechanisms of FcMeOH that can be considered: 1) As the anode ink is prepared, FcMeOH can be protonated by succinic acid (dicarboxylic acid) used for stabilisation of enzymes. This reaction leads to elimination of the hydroxyl group from FcMeOH forming an α -ferrocenyl carbocation [98], which can further form new species or even denature GOx. 2) Ferrocene can be oxidised to ferrocenium cation which is unstable in the presence of dioxygen and water [99], [100]. This leads to formation of insoluble species. 3) Thermal decomposition of ferrocene due to heating [101].

Operational stability could be increased with suitable cell design, ensuring good electrical and ionic contacts between adjacent surfaces. This was achieved by adding SAP on the anode side, preventing the leakage of electrolyte and delamination of the cathode. In order to have good conductivity in both in-plane and cross-plane directions, the adhesion of printed layers is also very important. This was achieved by tailoring inks with chitosan, a more hydrophobic polymer than PEO.

It is important to study operational stability between enzyme-mediator pairs. The ALDH/TMPD pair appeared to be rather unstable, although the stability of the ThL/ABTS pair was very good on ALDH anodes. This was most probably due to the fact that no H_2O_2 is formed at the anode when ALDH is used. Since GOx is used in aerobic conditions, H_2O_2 is formed which degrades the laccase cathode [102]. FcMeOH can also react with H_2O_2 , forming hydroxyl radicals and hydroxide ions via Fenton's chemistry, which again degrades the cells. Removing H_2O_2 from the anode by e.g. adding catalase could most probably stabilise the cells as reported in [103]. However, if dioxygen could be removed from the anode side, it would most probably stabilise both the enzyme and mediator.

5.3 Mass-manufacturing

Printing of enzymatic inks can be accomplished in mass-manufacturing. In order to move from laboratory scale rod- or screen-printing to rotary screen-printing, the enzymatic inks must be tailored to obtain certain characteristics. First of all, the inks must be homogenous and preferably thixotropic in order to maintain good ink flow on the screen. The rheological parameters of the ink can be tailored with solvents and binders. For example, the viscosity of water is ca. 1 cP, whereas for PEO (5 wt.% in H_2O) it is 8800-17600 cP and for medium molecular weight chitosan (1 wt.% in 1% acetic acid) 200-800 cP.

Adhesion between the ink and the printing substrate can be tailored either by selecting a substrate with surface free energy higher than the ink's surface tension (for water 72 mN m^{-1}) or by lowering the ink's surface tension. In this work, either cellulose- or carbon-based substrates were used. Surface tension of the ink was tailored with binders; the surface free energy of e.g. PEO is ca. 43 mN m^{-1} .

Drying of printed layers is a crucial step in R2R manufacturing. If the ink is still moist as the roll is wound after printing, the ink layer is destroyed. However, because delicate active components are used in the inks, over-drying them is also undesirable. Therefore, enzymatic inks need to be studied in terms of their heat tolerance. GOx and laccase appeared to tolerate heating very well.

If large-scale manufacturing of full biobatteries is the aim, at least six important steps must be considered: 1) mixing of the inks on demand; 2) printing and drying of the current collector layers on the substrate; 3) printing and drying of both the anode and cathode layers on the current collectors; 4) printing of an adhesive electrolyte-membrane hybrid on the top of the anodes and laminating the cathode side on it; 5) hot-pressing individual cells; and 6) cutting of individual cells.

The material costs of large-scale manufacturing are strongly dependent on the price of carbon, enzymes, and mediators, whereas paper-based substrates and polymers are available at a reasonable price. For example, the pilot-manufactured cells had an electrode area of 9 cm^2 and the dry matter content of each print was about 8 mg cm^{-2} . If the amount of the anode mediator is increased as suggested in the previous section, each electrode will contain approximately 1 mg of mediator. The enzyme amount should then be ca. 100 nkat. Commercial FcMeOH and ABTS cost around 50-60 € g^{-1} and enzymes 1-3 € kU^{-1} , meaning a total of 0.1-0.2 € per cell. Commercial CB-based inks can cost 1 $\text{€ g}^{-1}_{\text{ink}}$ and typical coverage is $100 \text{ cm}^2 \text{ g}^{-1}_{\text{ink}}$, which adds 0.18 € per cell. Therefore, developing in-house made inks is important because it can lower the overall

costs. These costs apply naturally to small batches only; with larger amounts the costs are expected to be significantly lower.

Considering environmental aspects, each individual chemical should be studied as well as their possible side reactions. In this thesis, some chemicals were rejected due to their toxicity, although they performed well. An example is MWCNTs, because handling them requires very careful safety procedures. The use of osmium-complexes as mediators was successful especially with ALDH, but they were rejected due to their possible high toxicity and poor availability.

5.4 Comparison to other flexible EBFCs

Over the past few years, many research groups have started developing bendable and wearable EBFCs (Table 10). As an example, the highest P_{\max} (0.12 mW cm^{-2} at 0.4 V) of single paper-based EBFC was reported with electrodes manufactured using GOx and BOD enzymes [104]. The highest power pulse (1.07 mW cm^{-2} with 4 mA cm^{-2} discharge current) was achieved with an EBFC/supercapacitor hybrid using GDH and BOD enzymes [105]. EBFCs constructed using fabrics have also been reported. The highest P_{\max} (0.95 mW cm^{-2} at 0.36 V) was achieved with a fructose dehydrogenase (FDH)/BOD cell [106]. A stack of three cells generated almost threefold higher power density (2.55 mW cm^{-2} at 1.21 V) than a single cell. Jia et al. [107] demonstrated the use of lactate oxidase (LOx)/Pt-black cells on fabrics for powering electronics with human sweat ($P_{\max} = 0.1 \text{ mW cm}^{-2}$ at 0.34 V). Multiple cells were printed on different garments for generating power for e.g. a LED or a digital watch during physical exercise.

Stretchable EBFCs have been developed and characterised on skin as epidermal patches for energy harvesting from sweat and even for wound healing and transdermal drug delivery. As examples, Ogawa et al. [108] demonstrated successful iontophoretic delivery of ascorbyl glucoside (used in anti-ageing treatments) through abdominal human skin using a commercial flow-through diffusion cell containing an enzyme cathode and anode. In another experiment, EBFC patches containing the fluorescent molecule rhodamine B (RB, 479 Da) were used on pigskin. When an iontophoretic current was applied (ca. $50 \mu\text{A cm}^{-2}$) using the patch for 1 h, the penetration of RB under the anode was obviously enhanced as compared to the penetration under the cathode. The amount of RB penetration was increased by longer treatment for 6 h, or by applying a higher current (ca. $80 \mu\text{A cm}^{-2}$) for 1 h. Tsubota et al. [109] demonstrated the use of an EBFC plaster for wound healing (on mouse skin), showing faster wound healing with the EBFC plaster than with a control plaster.

All the EBFCs mentioned here contain high surface area carbon materials, typically MWCNTs. The highest OCV and P_{\max} were reported with mediator-less FDH/BOD EBFC fabricated on MWCNT-modified carbon fabric. The highest power pulse was generated with an EBFC/supercapacitor hybrid fabricated using carbon paper and buckypaper. The reason why the printed EBFCs presented in this thesis do not show such high power densities can be attributed to the lack of high surface area carbon materials and the low amounts of enzymes and mediators on the electrodes. For example, the EBFCs reported in this section contained tens or even hundreds of enzyme units per each electrode. The electrodes manufactured at VTT contain ca. 1-5 U of enzyme per electrode. In addition, the use of mediators brings mass transport limitations as well as challenges with stability compared to mediator-less EBFCs. Using 1000-fold amounts of enzymes, striving for mediator-less systems and utilising high surface area carbon support could lead to a printed glucose/air biobattery/supercapacitor system that can perform steadily on the mW scale.

Table 10. Different bendable and wearable EBFCs.

Paper-based EBFCs	Fuel	Anode/Mediator	Cathode	Carbon	OCV	P_{max}
Publications II and III (laboratory manufacturing)	glucose	ALDH/Os(bpy) ₂ Cl ₂ (ca. 0.06 U cm ⁻²)	ThL/ABTS (ca. 0.06 U cm ⁻²)	DuPont ink MWCNT	0.62 V	3.5 μ W cm ⁻² (at 0.32 V)
Publication IV (laboratory manufacturing)	glucose	GOx/Fc/MeOH (ca. 0.3 U cm ⁻²)	ThL/ABTS (ca. 0.3 U cm ⁻²)	graphite	0.38 V	1.4 μ W cm ⁻² (at ca. 0.22 V)
Publications V and VI (pilot manufacturing)	glucose	GOx/Fc/MeOH (0.7-0.9 U cm ⁻²)	Ecol/ABTS (ca. 0.8 U cm ⁻²)	graphite	0.37 V	0.63 μ W cm ⁻² (at ca. 0.2 V)
Zhang et al. [110]	glucose NAD ⁺	GDH	BOD	MWCNT ^a	0.56 V	13.5 μ W cm ⁻² (at 0.33 V)
Shitanda et al. [104]	glucose	GOx/TTF ^b (400 U cm ⁻²)	BOD (20 U cm ⁻²)	Keijenblack	0.55 V	0.12 mW cm ⁻² (at 0.4 V)
Wu et al. [111]	fructose	FDH (0.1 mg)	BOD (0.1 mg)	MWCNT	0.61 V	4.31 μ W (at ca. 0.4 V)
Lau et al. [112]	ethanol NAD ⁺	ADH ^c +AIDH ^d /PMG ^e (100 U cm ⁻² of each enzyme)	BOD (10 U cm ⁻²)	MWCNT ^f	0.53 V	35.5 μ W cm ⁻² (at ca. 0.4 V)
Lau et al. [112]	methanol formaldehyde formic acid NAD ⁺	ADH+AIDH ^g +FoDH ^h /PMG (10 U cm ⁻² of each enzyme)	BOD (10 U cm ⁻²)	MWCNT ^f	0.55 V	26.9 μ W cm ⁻² (at ca. 0.38 V)
Narvaez Villarrubia et al. [105]	glucose	GDH/MG ^h (9.93 mg)	BOD (80 mg)	Buckypaper	0.56 V	1.07 mW cm ⁻² (a pulse of 4 mA cm ⁻²)

	Fuel	Anode/Mediator	Cathode	Carbon	OCV	P_{max}
Fabric-based EBFCs						
Haneda et al. [113]	fructose (in agarose film)	FDH (3400 U cm ⁻²)	BOD (5 U cm ⁻²)	MWCNT Ketjenblack	0.70 V	0.55 mW cm ⁻² (at 0.4 V)
Miyake et al. [106]	fructose	FDH	BOD	MWCNT	0.74 V	0.95 mW cm ⁻² (at 0.36 V)
Miyake et al. [106] (triple cell)	fructose	FDH	BOD	MWCNT	2.09 V	2.55 mW cm ⁻² (at 1.21 V)
Jia et al. [107]	lactate	LOx+BSA/TTF-TCNQ ^l	Pt-black	CNT	0.67 V	100 μ W cm ⁻² (at 0.34 V)
Stretchable EBFCs for skin						
Bandodkar et al. [114]	glucose	GOx+BSA/NQ ^k	Pt	MWCNT	ca. 0.4 V	ca. 125 μ W cm ⁻² (at ca. 0.28 V)
Jia et al. [115]	lactate	LOx+BSA/TTF (ca. 16 U μ electrode)	Pt black	MWCNT	ca. 0.5 V	44 μ W cm ⁻² (at ca. 0.29 V)
Ogawa et al. [116]	fructose (in hydrogel film)	FDH	BOD	MWCNT SWCNT	0.74 V	0.25 mW cm ⁻² (at ca. 0.4 V)
Ogawa et al. [108] (transdermal drug delivery)	fructose (in hydrogel film)	FDH	BOD	MWCNT	0.75 V (on pig-skin)	60 μ W cm ⁻² (at ca. 0.3 V on pigskin)
Tsubota et al. [109] (wound healing)	fructose (in gel film)	FDH	BOD	CNT	ca. 0.75 V	(0.4 mA cm ⁻² constant current for 12 h around a wound on a mouse skin)

^a functionalised with ionic liquid, ^b TTF = tetrathiafulvalene, ^c ADH = alcohol dehydrogenase, ^d AIDH = aldehyde dehydrogenase, ^e PMG = polymethylene green, ^f coated with PMG, ^g FodH = formate dehydrogenase, ^h MIG = methylene green, ⁱ BSA = bovine serum albumin, ^j TCNQ = 7,7,8,8-tetracyanoquinodimethane, ^k NQ = 1,4-naphthoquinone

5.5 Suggestions for future research and development

Roughly 20 years ago, Palmore and Whitesides [31] suggested that the future work on BFCs should concentrate on the following question: "Is the activity available in biological catalysts sufficient, and in the right form, to provide the basis for a practical fuel cell?" This thesis work has proven that yes, EBFCs can provide sufficient amount of power for practical applications. However, there is still work to be done in the future in order to develop these biobatteries further:

- There is a need to study more the possible degradation processes of the cell. As this thesis work showed, both the enzymes and mediators degrade during the manufacturing, storing and use. The printed layers were also delaminating from the current collectors, which may be due to the degradation of the polymers in the inks. In order to optimise these cells, better understanding on degradation processes between the used chemical species is needed.
- More loss analysis of the system is needed to discover the restricting processes in the cell. Especially in the case of a mediated system, it is important to establish the rate limiting steps in the transfer of electrons from the mediator to the electrode surface and to determine the relevant mass transport and enzyme kinetic rates. Without these values, optimal design of 3D electrode structures cannot be achieved.
- Mass transfer characteristics of the 3D electrodes could be enhanced by patterned printing. Both hydrophobic and hydrophilic channels could be created forming a functional matrix. For an example, air cathodes need channels both for liquid and gas phase species.
- Optimisation of the cell structure should take into account that the anode should be free from oxygen, but at the same time, that is the fuel for the cathode. Drying of these cells is also problematic. For this reason, ways to prevent the electrolyte leakage or evaporation are needed.
- Exploring the possibility to use a multivariable management technique particularly for the mass production of these flexible biobatteries is essential. As some of the depositing techniques used in this thesis may need to be revised and changed, it can bring complexity to the manufacturing process.

6. Summary and conclusions

This thesis studied the possibility of manufacturing printed enzymatic biobatteries in large scale. The performance of laboratory-manufactured cells was compared to pilot-manufactured biobatteries. The selection of suitable enzyme-mediator pairs as well as binders and the carbon support of the enzymatic inks has significant effect on the biobattery performance and stability.

The anode and cathode were chosen to contain GOx/FcMeOH and high potential laccase/ABTS pairs, respectively. Although the ALDH enzyme performed very well on the anode, it was rejected due to its poor availability and stability. The stability in manufacturing, storage and during use should all be considered when an application of biobatteries for consumer products is planned. Immobilisation and stabilisation of both enzymes and mediators must be taken into account in order to maintain good performance.

The activity of enzymes could be maintained at 60-80% even though the enzymatic layers were dried at high temperatures and stored for one month at room temperature. However, when mediators were added into the inks, the degradation of enzymes was faster, and only 20-30% on the enzymatic activity was maintained after storing for one month. Therefore, the stabilisation of mediators should be studied in more detail in the future. The possibility of mediator-less electrodes, especially for the cathode side, seems plausible. This approach would increase the stability of the cell. Another suggestion is to add catalase to the anode side to remove H_2O_2 . This could improve the operational stability of the biobatteries.

Applications that could benefit from this kind of batteries are disposable sensors or memory devices that are used for a few days at room temperature. At the moment, these printed biobatteries have demonstrated maximum power densities in the range of 1-3 $\mu W\ cm^{-2}$ and maximum energy outputs ($E_{cut-off} = 200\ mV$) in the range of 10-20 $\mu Wh\ cm^{-2}$. A battery the size of a credit card (ca. 50 cm^2) could generate 50-150 μW or 0.5-1 mWh. This level of power suffices for e.g. smart RFID tags or low energy Bluetooth in idle mode (some μAs). However, in active mode they need 10-15 mA current at ca. 2 V for waking up and transmitting data to a master receiver. This would require at least three biobatteries connected in series or a converter to boost the output voltage. In order to improve peak power generation, the integration of biobatteries with supercapacitors is recommended. Other suitable applications of biobatteries could be water leakage detection, cold chain detection (especially for frozen goods), and autonomous biosensors. Furthermore, other applications could also include microcurrent patches for skin and wounds if the power generation of printed biobatteries could be increased from μW scale to mW scale.

Bibliography

- [1] M. Hilder, B. Winther-Jensen, and N. B. Clark, "Paper-based, printed zinc-air battery," *J. Power Sources*, vol. 194, no. 2, pp. 1135–1141, Dec. 2009.
- [2] K. T. Braam, S. K. Volkman, and V. Subramanian, "Characterization and optimization of a printed, primary silver-zinc battery," *J. Power Sources*, vol. 199, pp. 367–372, 2012.
- [3] A. M. Gaikwad, D. a. Steingart, T. Nga Ng, D. E. Schwartz, and G. L. Whiting, "A flexible high potential printed battery for powering printed electronics," *Appl. Phys. Lett.*, vol. 102, no. 23, p. 233302, 2013.
- [4] K. Fu, Y. Wang, C. Yan, Y. Yao, Y. Chen, J. Dai, S. Lacey, Y. Wang, J. Wan, T. Li, Z. Wang, Y. Xu, and L. Hu, "Graphene Oxide-Based Electrode Inks for 3D-Printed Lithium-Ion Batteries," *Adv. Mater.*, vol. 28, no. 13, pp. 2587–2594, 2016.
- [5] S. Suren and S. Kheawhom, "Development of a High Energy Density Flexible Zinc-Air Battery," *J. Electrochem. Soc.*, vol. 163, no. 6, pp. A846–A850, 2016.
- [6] A. T. Yahiro, S. M. Lee, and D. O. Kimble, "Enzyme utilizing bio-fuel cell studies," *Biochim. Biophys. Acta*, vol. 88, pp. 375–383, 1964.
- [7] G. T. R. Palmore, H. Bertschy, S. H. Bergens, and G. M. Whitesides, "A methanol/dioxygen biofuel cell that uses NAD⁺-dependent dehydrogenases as catalysts: application of an electro-enzymatic method to regenerate nicotinamide adenine dinucleotide at low overpotentials," *J. Electroanal. Chem.*, vol. 443, pp. 155–161, 1998.
- [8] P. K. Addo, R. L. Arechederra, and S. D. Minteer, "Evaluating enzyme cascades for methanol/air biofuel cells based on NAD⁺-dependent enzymes," *Electroanalysis*, vol. 22, no. 7–8, pp. 807–812, 2010.
- [9] R. L. Arechederra and S. D. Minteer, "Complete Oxidation of Glycerol in an Enzymatic Biofuel Cell," *Fuel Cells*, vol. 9, no. 1, pp. 63–69, 2009.
- [10] D. Sokic-Lazic and S. D. Minteer, "Citric acid cycle biomimic on a carbon electrode," *Biosens. Bioelectron.*, vol. 24, no. 4, pp. 939–944, 2008.
- [11] S. Xu and S. D. Minteer, "Enzymatic Biofuel Cell for Oxidation of Glucose to CO₂," *ACS Catal.*, vol. 2, no. 1, pp. 91–94, 2012.
- [12] D. P. Hickey, F. Giroud, D. W. Schmidtke, D. T. Glatzhofer, and S. D. Minteer, "Enzyme cascade for catalyzing sucrose oxidation in a biofuel cell," *ACS Catal.*, vol. 3, no. 12, pp. 2729–2737, 2013.
- [13] A. Heller, "Electrical wiring of redox enzymes," *Acc. Chem. Res.*, vol. 23, no. 5, pp. 128–134, 1990.
- [14] T. Chen, S. C. Barton, G. Binyamin, Z. Gao, Y. Zhang, H.-H. Kim, and A. Heller, "A miniature biofuel cell," *J. Am. Chem. Soc.*, vol. 123, no. 35, pp. 8630–8631, 2001.
- [15] N. Mano, F. Mao, and A. Heller, "Characteristics of a Miniature Compartment-less Glucose-O₂ Biofuel Cell and Its Operation in a Living Plant," *J. Am. Chem. Soc.*, vol. 125, no. 21, pp. 6588–6594, 2003.
- [16] L. Halámková, J. Haláček, V. Bocharova, A. Szczupak, L. Alfonta, and E. Katz, "Implanted biofuel cell operating in a living snail," *J. Am. Chem. Soc.*, vol. 134, no. 11, pp. 5040–5043, 2012.
- [17] A. Szczupak, J. Haláček, L. Halámková, V. Bocharova, L. Alfonta, and E. Katz, "Living battery – biofuel cells operating in vivo in clams," *Energy Environ. Sci.*, vol. 5, no. 10, p. 8891, 2012.
- [18] M. Southcott, K. MacVittie, J. Haláček, L. Halámková, W. D. Jemison, R. Lobel, and E. Katz, "A pacemaker powered by an implantable biofuel cell operating under conditions mimicking the human

- blood circulatory system--battery not included.," *Phys. Chem. Chem. Phys.*, vol. 15, no. 17, pp. 6278–83, 2013.
- [19] E. Katz, A. Bückmann, and I. Willner, "Self-powered enzyme-based biosensors," *J. Am. Chem. Soc.*, vol. 123, pp. 10752–10753, 2001.
- [20] K. MacVittie and E. Katz, "Self-powered electrochemical memristor based on a biofuel cell--towards memristors integrated with biocomputing systems.," *Chem. Commun. (Camb)*, vol. 50, no. 37, pp. 4816–9, 2014.
- [21] Y. Wang, L. Ge, P. Wang, M. Yan, J. Yu, and S. Ge, "A three-dimensional origami-based immuno-biofuel cell for self-powered, low-cost, and sensitive point-of-care testing," *Chem. Commun.*, vol. 50, no. 16, p. 1947, 2014.
- [22] P. Atanassov, C. Applett, S. Banta, S. Brozik, S. Calabrese Barton, M. Cooney, B. Y. Liaw, S. Mukerjee, and S. D. Minteer, "Enzymatic biofuel cells," *Electrochem. Soc. Interface*, vol. 16, pp. 28–31, 2007.
- [23] A. Heller, "Miniature biofuel cells," *Phys. Chem. Chem. Phys.*, vol. 6, no. 2, p. 209, 2004.
- [24] M. Rasmussen, S. Abdellaoui, and S. D. Minteer, "Enzymatic biofuel cells: 30 years of critical advancements," *Biosens. Bioelectron.*, vol. 76, pp. 91–102, 2016.
- [25] A. J. Bandodkar and J. Wang, "Wearable Biofuel Cells: A Review," *Electroanalysis*, vol. 28, no. 6, pp. 1188–1200, 2016.
- [26] M. J. Moehlenbrock and S. D. Minteer, "Extended lifetime biofuel cells," *Chem. Soc. Rev.*, vol. 37, no. 6, pp. 1188–1196, 2008.
- [27] A. Illanes, "Stability of biocatalysts," *Electron. J. Biotechnol.*, vol. 2, no. 1, pp. 7–15, 1999.
- [28] U. T. Bornscheuer, "Immobilizing enzymes: How to create more suitable biocatalysts," *Angew. Chemie - Int. Ed.*, vol. 42, no. 29, pp. 3336–3337, 2003.
- [29] K. M. Polizzi, A. S. Bommarius, J. M. Broering, and J. F. Chaparro-Riggers, "Stability of biocatalysts," *Curr. Opin. Chem. Biol.*, vol. 11, no. 2, pp. 220–5, Apr. 2007.
- [30] U. Hanefeld, L. Gardossi, and E. Magner, "Understanding enzyme immobilisation," *Chem Soc Rev*, vol. 38, no. 2, pp. 453–468, 2009.
- [31] G. T. R. Palmore and G. M. Whitesides, "Microbial and Enzymatic Biofuel Cells," in *Enzymatic Conversion of Biomass for Fuels Production*, M. E. Himmel, J. O. Baker, and R. P. Overend, Eds. American Chemical Society, 1994, pp. 271–290.
- [32] S. Calabrese Barton, J. Gallaway, and P. Atanassov, "Enzymatic Biofuel Cells for Implantable and Microscale Devices," *Chem. Rev.*, vol. 104, no. 10, pp. 4867–4886, Oct. 2004.
- [33] M. J. Cooney, V. Svoboda, C. Lau, G. Martin, and S. D. Minteer, "Enzyme catalysed biofuel cells," *Energy Environ. Sci.*, vol. 1, no. 3, pp. 320–337, 2008.
- [34] S. D. Minteer, B. Y. Liaw, and M. J. Cooney, "Enzyme-based biofuel cells.," *Curr. Opin. Biotechnol.*, vol. 18, no. 3, pp. 228–34, Jun. 2007.
- [35] G. M. Cooper, *The Cell: A Molecular Approach*, 2nd ed. Sunderland (MA): Sinauer Associates Inc., 2000.
- [36] O. H. Hashim and N. A. Adnan, "Coenzyme, cofactor and prosthetic group — Ambiguous biochemical jargon," *Biochem. Educ.*, vol. 22, no. 2, pp. 93–94, 1994.
- [37] C. O. Fagain, "Understanding and increasing protein stability," *Biochim. Biophys. Acta - Protein Struct. Mol. Enzymol.*, vol. 1252, no. 1, pp. 1–14, 1995.

- [38] S. Ferri, K. Kojima, and K. Sode, "Review of glucose oxidases and glucose dehydrogenases: a bird's eye view of glucose sensing enzymes.," *J. Diabetes Sci. Technol.*, vol. 5, no. 5, pp. 1068–76, 2011.
- [39] R. Wilson and A. Turner, "Glucose oxidase: an ideal enzyme," *Biosens. Bioelectron.*, vol. 7, pp. 165–185, 1992.
- [40] V. Leskovac, S. Trivić, G. Wohlfahrt, J. Kandrač, and D. Peričin, "Glucose oxidase from *Aspergillus niger*: The mechanism of action with molecular oxygen, quinones, and one-electron acceptors," *Int. J. Biochem. Cell Biol.*, vol. 37, no. 4, pp. 731–750, 2005.
- [41] M. Meyer, G. Wohlfahrt, J. Knäblein, and D. Schomburg, "Aspects of the mechanism of catalysis of glucose oxidase: a docking, molecular mechanics and quantum chemical study.," *J. Comput. Aided. Mol. Des.*, vol. 12, no. 5, pp. 425–40, Sep. 1998.
- [42] X. Zhang, D. Liu, L. Li, and T. You, "Direct Electrochemistry of Glucose Oxidase on Novel Free-Standing Nitrogen-Doped Carbon Nanospheres@Carbon Nanofibers Composite Film," *Sci. Rep.*, vol. 5, p. 9885, 2015.
- [43] X. Wu, F. Zhao, J. R. Varcoe, A. E. Thumser, C. Avignone-Rossa, and R. C. T. Slade, "Direct electron transfer of glucose oxidase immobilized in an ionic liquid reconstituted cellulose-carbon nanotube matrix.," *Bioelectrochemistry*, vol. 77, no. 1, pp. 64–8, Nov. 2009.
- [44] M. Zhao, Y. Gao, J. Sun, and F. Gao, "Mediatorless Glucose Biosensor and Direct Electron Transfer Type Glucose/Air Biofuel Cell Enabled with Carbon Nanodots," *Anal. Chem.*, vol. 87, pp. 2615–2622, 2015.
- [45] D. Ivnitski, K. Artyushkova, R. a. Rincón, P. Atanassov, H. R. Luckarift, and G. R. Johnson, "Entrapment of enzymes and carbon nanotubes in biologically synthesized silica: Glucose oxidase-catalyzed direct electron transfer," *Small*, vol. 4, no. 3, pp. 357–364, 2008.
- [46] H. J. Hecht, H. M. Kalisz, J. Hendle, R. D. Schmid, and D. Schomburg, "Crystal structure of glucose oxidase from *Aspergillus niger* refined at 2.3 Å resolution.," *J. Mol. Biol.*, vol. 229, no. 1, pp. 153–172, 1993.
- [47] J. Buchert, "A xylose-oxidizing membrane-bound aldose dehydrogenase of *Gluconobacter oxydans* ATCC 621," *J. Biotechnol.*, vol. 18, pp. 103–113, 1991.
- [48] A. Oubrie, H. J. Rozeboom, K. H. Kalk, A. J. Olsthoorn, J. A. Duine, and B. W. Dijkstra, "Structure and mechanism of soluble quinoprotein glucose dehydrogenase.," *EMBO J.*, vol. 18, no. 19, pp. 5187–94, Oct. 1999.
- [49] M. Yamada, K. Matsushita, C. T. Migita, and O. Adachi, "Escherichia coli PQQ-containing quinoprotein glucose dehydrogenase: its structure comparison with other quinoproteins," *Biochim. Biophys. Acta*, vol. 1647, pp. 185–192, 2003.
- [50] C. Anthony, "Pyrroloquinoline quinone (PQQ) and quinoprotein enzymes.," *Antioxid. Redox Signal.*, vol. 3, no. 5, pp. 757–74, Oct. 2001.
- [51] Y. Ohshiro and S. Itoh, "The Chemistry of PQQ and Related Compounds," in *Principles and Applications of Quinoproteins*, V. L. Davidson, Ed. New York: Marcel Dekker, Inc., 1993, pp. 309–329.
- [52] S. Babanova, I. Matanovic, and P. Atanassov, "Quinone-Modified Surfaces for Enhanced Enzyme-Electrode Interactions in Pyrroloquinoline-Quinone-Dependent Glucose Dehydrogenase Anodes," *ChemElectroChem*, vol. 1, no. 11, pp. 2017–2028, 2014.
- [53] D. Ivnitski, P. Atanassov, and C. Apblett, "Direct bioelectrocatalysis of PQQ-dependent glucose dehydrogenase," *Electroanalysis*, vol. 19, no. 15, pp. 1562–1568, 2007.
- [54] V. Flexer and N. Mano, "Wired pyrroloquinoline quinone soluble glucose dehydrogenase enzyme

- electrodes operating at unprecedented low redox potential.," *Anal. Chem.*, vol. 86, no. 5, pp. 2465–73, 2014.
- [55] V. Flexer, F. Durand, S. Tsujimura, and N. Mano, "Efficient direct electron transfer of PQQ-glucose dehydrogenase on carbon cryogel electrodes at neutral pH.," *Anal. Chem.*, vol. 83, no. 14, pp. 5721–7, Jul. 2011.
- [56] A. R. Dewanti and J. A. Duine, "Reconstitution of Membrane-Integrated Quinoprotein Glucose Dehydrogenase Apoenzyme with PQQ and the Holoenzyme's Mechanism of Action," *Biochemistry*, vol. 37, no. 19, pp. 6810–6818, 1998.
- [57] A. Oubrie, H. J. Rozeboom, K. H. Kalk, J. A. Duine, and B. W. Dijkstra, "The 1.7 Å crystal structure of the apo form of the soluble quinoprotein glucose dehydrogenase from *Acinetobacter calcoaceticus* reveals a novel internal conserved sequence repeat.," *J. Mol. Biol.*, vol. 289, no. 2, pp. 319–333, 1999.
- [58] M. Ameyama and E. Shinagawa, "D-Glucose dehydrogenase of *Gluconobacter suboxydans*: solubilization, purification and characterization," *Agric. Biol. Chem. Biol. Chem.*, vol. 45, no. 4, pp. 851–861, 1981.
- [59] M. Frascioni, H. Boer, A. Koivula, and F. Mazzei, "Electrochemical evaluation of electron transfer kinetics of high and low redox potential laccases on gold electrode surface," *Electrochim. Acta*, vol. 56, no. 2, pp. 817–827, Dec. 2010.
- [60] A. Christenson, S. Shleev, N. Mano, A. Heller, and L. Gorton, "Redox potentials of the blue copper sites of bilirubin oxidases," *Biochim. Biophys. Acta - Bioenerg.*, vol. 1757, no. 12, pp. 1634–1641, 2006.
- [61] E. I. Solomon, U. M. Sundaram, and T. E. Machonkin, "Multicopper oxidases and oxygenases," *Chem. Rev.*, vol. 96, no. 7, pp. 2563–2605, 1996.
- [62] E. I. Solomon, P. Chen, M. Metz, S.-K. Lee, and A. E. Palmer, "Oxygen Binding, Activation, and Reduction to Water by Copper Proteins.," *Angew. Chem. Int. Ed. Engl.*, vol. 40, no. 24, pp. 4570–4590, Dec. 2001.
- [63] S. Shleev, A. Jarosz-Wilkolazka, A. Khalunina, O. Morozova, A. Yaropolov, T. Ruzgas, and L. Gorton, "Direct electron transfer reactions of laccases from different origins on carbon electrodes.," *Bioelectrochemistry*, vol. 67, no. 1, pp. 115–24, Sep. 2005.
- [64] N. Hakulinen and J. Rouvinen, "Three-dimensional structures of laccases," *Cell. Mol. Life Sci.*, vol. 72, no. 5, pp. 857–868, 2015.
- [65] P. Baldrian, "Fungal laccases - occurrence and properties.," *FEMS Microbiol. Rev.*, vol. 30, no. 2, pp. 215–42, Mar. 2006.
- [66] N. Hakulinen, K. Kruus, A. Koivula, and J. Rouvinen, "A crystallographic and spectroscopic study on the effect of X-ray radiation on the crystal structure of *Melanocarpus albomyces* laccase," *Biochem. Biophys. Res. Commun.*, vol. 350, pp. 929–934, 2006.
- [67] V. Madhavi and S. S. Lele, "Laccase: properties and applications," *BioResources*, vol. 4, no. 4, pp. 1694–1717, 2009.
- [68] A. M. Mayer and R. C. Staples, "Laccase: New functions for an old enzyme," *Phytochemistry*, vol. 60, no. 6, pp. 551–565, 2002.
- [69] S. Riva, "Laccases: blue enzymes for green chemistry," *Trends Biotechnol.*, vol. 24, no. 5, pp. 219–226, 2006.
- [70] H. Claus, "Laccases: Structure, reactions, distribution," *Micron*, vol. 35, no. 1–2, pp. 93–96, 2004.
- [71] U. N. Dwivedi, P. Singh, V. P. Pandey, and A. Kumar, "Structure-function relationship among

- bacterial, fungal and plant laccases,” *J. Mol. Catal. B Enzym.*, vol. 68, no. 2, pp. 117–128, 2011.
- [72] M. Frascioni, G. Favero, H. Boer, A. Koivula, and F. Mazzei, “Kinetic and biochemical properties of high and low redox potential laccases from fungal and plant origin.,” *Biochim. Biophys. Acta*, vol. 1804, no. 4, pp. 899–908, Apr. 2010.
- [73] J. R. Winkler and H. B. Gray, “Long-Range Electron Tunneling,” *J. Am. Chem. Soc.*, vol. 136, no. 8, pp. 2930–2939, 2014.
- [74] S. Mayo, W. Ellis, R. Crutchley, and H. Gray, “Long-range electron transfer in heme proteins,” *Science (80-.)*, vol. 233, no. 4767, pp. 948–952, 1986.
- [75] Y. Degani and a Heller, “Direct Electrical Communication between Chemically Modified Enzymes and Metal Electrodes,” *J. Phys. Chem.*, vol. 91, no. 6, pp. 1287–9, 1987.
- [76] M. Smolander, G. Marko-Varga, and L. Gorton, “Aldose dehydrogenase-modified carbon paste electrodes as amperometric aldose sensors,” *Anal. Chim. Acta*, vol. 302, pp. 233–240, 1995.
- [77] A. Le Goff, M. Holzinger, and S. Cosnier, “Recent progress in oxygen-reducing laccase biocathodes for enzymatic biofuel cells,” *Cell. Mol. Life Sci.*, vol. 72, no. 5, pp. 941–952, 2015.
- [78] S. Shleev, J. Tkac, A. Christenson, T. Ruzgas, A. I. Yaropolov, J. W. Whittaker, and L. Gorton, “Direct electron transfer between copper-containing proteins and electrodes,” *Biosens. Bioelectron.*, vol. 20, no. 12, pp. 2517–2554, 2005.
- [79] X. Wang, R. Latonen, P. Sjöberg-Eerola, J.-E. Eriksson, J. Bobacka, H. Boer, and M. Bergelin, “Direct electron transfer of *Trametes hirsuta* laccase in a dual-layer architecture of poly (3, 4-ethylenedioxythiophene) films,” *J. Phys. Chem. C*, vol. 115, pp. 5919–5929, 2011.
- [80] J. W. Gallaway and S. A. C. Barton, “Kinetics of redox polymer-mediated enzyme electrodes,” *J. Am. Chem. Soc.*, vol. 130, no. 26, pp. 8527–8536, 2008.
- [81] C. Bourdillon, C. Demaille, J. Moiroux, and J. Savéant, “Catalysis and mass transport in spatially ordered enzyme assemblies on electrodes,” *J. Am. Chem. Soc.*, vol. 117, pp. 11499–11506, 1995.
- [82] N. Perez, “Mass Transport by Diffusion and Migration,” in *Electrochemistry and Corrosion Science*, Springer International Publishing Switzerland, 2016, pp. 151–197.
- [83] M. J. Moehlenbrock, R. L. Arechederra, K. H. Sjöholm, and S. D. Minteer, “Analytical techniques for characterizing enzymatic biofuel cells,” *Anal. Chem.*, vol. 81, no. 23, pp. 9538–9545, 2009.
- [84] A. Dwevedi, “Basics of Enzyme Immobilization,” in *Enzyme Immobilization*, Springer International Publishing Switzerland, 2016, pp. 21–45.
- [85] T. Klotzbach, M. Watt, Y. Ansari, and S. D. Minteer, “Effects of hydrophobic modification of chitosan and Nafion on transport properties , ion-exchange capacities , and enzyme immobilization,” *J. Memb. Sci.*, vol. 282, pp. 276–283, 2006.
- [86] J. B. Rosenholm, “Wetting of Surfaces and Interfaces: a Conceptual Equilibrium Thermodynamic Approach,” in *Colloid Stability: The Role of Surface Forces, Part II*, vol. 2, T. F. Tadros, Ed. Weinheim: WILEY-VCH Verlag GmbH & Co. KGaA, 2007, pp. 1–83.
- [87] K. Gilleo, “Rheology and Surface Chemistry for Screen Printing,” *Screenprinting*, no. February, pp. 128–132, 1989.
- [88] A. Falsafi, S. Mangibudi, and M. J. Owen, “Surface and Interfacial Properties,” in *Physical Properties of Polymers Handbook*, 2nd ed., J. E. Mark, Ed. Springer Science & Business Media, 2007.
- [89] H. Kautsky, “Quenching of luminescence by oxygen,” *Trans. Faraday Soc.*, vol. 35, pp. 216–219, 1939.
- [90] M. Fleischmann and J. N. Hiddleston, “A palladium-hydrogen probe electrode for use as a

- microreference electrode," *J. Phys. E.*, vol. 1, no. 2, pp. 667–668, 1968.
- [91] A. J. Bard and L. R. Faulkner, *Electrochemical Methods: Fundamentals and Applications*, 2nd ed. John Wiley & Sons, Inc, 2001.
- [92] R. Bourbonnais, D. Leech, and M. G. Paice, "Electrochemical analysis of the interactions of laccase mediators with lignin model compounds.," *Biochim. Biophys. Acta*, vol. 1379, no. 3, pp. 381–390, 1998.
- [93] A. Majcherczyk, C. Johannes, and A. Huttermann, "Oxidation of aromatic alcohols by laccase from *Trametes versicolor* mediated by the 2,2'-azino-bis-(3-ethylbenzothiazoline-6-sulphonic acid) cation radical and dication," *Appl. Microbiol. Biotechnol.*, vol. 51, no. 2, pp. 267–276, 1999.
- [94] C. Johannes, A. Majcherczyk, and C. Johannes, "Natural Mediators in the Oxidation of Polycyclic Aromatic Hydrocarbons by Laccase Mediator Systems Natural Mediators in the Oxidation of Polycyclic Aromatic Hydrocarbons by Laccase Mediator Systems," *Appl. Environ. Microbiol.*, vol. 66, no. 2, pp. 524–528, 2000.
- [95] M. Solís-Oba, V. M. Ugalde-Saldívar, I. González, and G. Viniestra-González, "An electrochemical-spectrophotometrical study of the oxidized forms of the mediator 2,2'-azino-bis-(3-ethylbenzothiazoline-6-sulfonic acid) produced by immobilized laccase," *J. Electroanal. Chem.*, vol. 579, no. 1, pp. 59–66, 2005.
- [96] S. Dong, H. Xiao, Q. Huang, J. Zhang, L. Mao, and S. Gao, "Graphene Facilitated Removal of Labetalol in Laccase-ABTS System: Reaction Efficiency, Pathways and Mechanism," *Sci. Rep.*, vol. 6, no. February, p. 21396, 2016.
- [97] Y. Tong, Y. Lin, S. Wang, and M. Song, "A study of crystallisation of poly(ethylene oxide) and polypropylene on graphene surface," *Polymer (Guildf.)*, vol. 73, pp. 52–61, 2015.
- [98] P. Peljo, L. Qiao, L. Murtomäki, C. Johans, H. H. Girault, and K. Kontturi, "Electrochemically controlled proton-transfer-catalyzed reactions at liquid-liquid interfaces: nucleophilic substitution on ferrocene methanol.," *Chemphyschem a Eur. J. Chem. Phys. Phys. Chem.*, vol. 14, no. 2, pp. 311–4, Feb. 2013.
- [99] J. P. Hurvois and C. Moinet, "Reactivity of ferrocenium cations with molecular oxygen in polar organic solvents: Decomposition, redox reactions and stabilization," *J. Organomet. Chem.*, vol. 690, pp. 1829–1839, 2005.
- [100] A. Singh, D. R. Chowdhury, and A. Paul, "A kinetic study of ferrocenium cation decomposition utilizing an integrated electrochemical methodology composed of cyclic voltammetry and amperometry," *Analyst*, vol. 139, pp. 5747–5754, 2014.
- [101] A. Bhattacharjee, A. Rooj, D. Roy, and M. Roy, "Thermal Decomposition Study of Ferrocene [(C₅H₅)₂Fe]," *J. Exp. Phys.*, vol. 2014, p. 8, 2014.
- [102] R. D. Milton, F. Giroud, A. E. Thumser, S. D. Minter, and R. C. T. Slade, "Hydrogen peroxide produced by glucose oxidase affects the performance of laccase cathodes in glucose/oxygen fuel cells: FAD-dependent glucose dehydrogenase as a replacement.," *Phys. Chem. Chem. Phys.*, vol. 15, no. 44, pp. 19371–9, 2013.
- [103] A. Zebda, C. Gondran, A. Le Goff, M. Holzinger, P. Cinquin, and S. Cosnier, "Mediatorless high-power glucose biofuel cells based on compressed carbon nanotube-enzyme electrodes.," *Nat. Commun.*, vol. 2, no. May, p. 370, Jan. 2011.
- [104] I. Shitanda, S. Kato, Y. Hoshi, M. Itagaki, and S. Tsujimura, "Flexible and high-performance paper-based biofuel cells using printed porous carbon electrodes.," *Chem. Commun.*, vol. 49, no. 94, pp. 11110–2, Dec. 2013.
- [105] C. W. Narvaez Villarrubia, F. Soavi, C. Santoro, C. Arbizzani, A. Serov, S. Rojas-Carbonell, G.

- Gupta, and P. Atanassov, "Self-feeding paper based biofuel cell/self-powered hybrid μ -supercapacitor integrated system," *Biosens. Bioelectron.*, vol. 86, pp. 459–465, 2016.
- [106] T. Miyake, K. Haneda, S. Yoshino, and M. Nishizawa, "Flexible, layered biofuel cells," *Biosens. Bioelectron.*, vol. 40, no. 1, pp. 45–49, 2013.
- [107] W. Jia, X. Wang, S. Imani, A. J. Bandodkar, J. Ramírez, P. P. Mercier, and J. Wang, "Wearable textile biofuel cells for powering electronics," *J. Mater. Chem. A*, vol. 2, no. 43, pp. 18184–18189, 2014.
- [108] Y. Ogawa, K. Kato, T. Miyake, K. Nagamine, T. Ofuji, S. Yoshino, and M. Nishizawa, "Organic Transdermal Iontophoresis Patch with Built-in Biofuel Cell," *Adv. Healthc. Mater.*, vol. 4, no. 4, pp. 506–510, 2015.
- [109] A. Tsubota, Y. Ogawa, T. Yamauchi, H. Kai, K. Yamasaki, and M. Nishizawa, "Development of a Therapeutic Device for Wound Healing with Enzymatic Biofuel Cells," *Electrochem. Soc.*, vol. Meeting Ab, no. 53, p. 3903, Sep. 2016.
- [110] L. Zhang, M. Zhou, D. Wen, L. Bai, B. Lou, and S. Dong, "Small-size biofuel cell on paper," *Biosens. Bioelectron.*, vol. 35, no. 1, pp. 155–159, May 2012.
- [111] X. E. Wu, Y. Z. Guo, M. Y. Chen, and X. D. Chen, "Fabrication of flexible and disposable enzymatic biofuel cells," *Electrochim. Acta*, vol. 98, pp. 20–24, 2013.
- [112] C. Lau, M. J. Moehlenbrock, R. L. Arechederra, A. Falase, K. Garcia, R. Rincon, S. D. Minter, S. Banta, G. Gupta, S. Babanova, and P. Atanassov, "Paper based biofuel cells: Incorporating enzymatic cascades for ethanol and methanol oxidation," *Int. J. Hydrogen Energy*, vol. 40, no. 42, pp. 14661–14666, 2015.
- [113] K. Haneda, S. Yoshino, T. Ofuji, T. Miyake, and M. Nishizawa, "Sheet-shaped biofuel cell constructed from enzyme-modified nanoengineered carbon fabric," *Electrochim. Acta*, vol. 82, pp. 175–178, 2012.
- [114] A. J. Bandodkar, I. Jeerapan, J. M. You, R. Nuñez-Flores, and J. Wang, "Highly Stretchable Fully-Printed CNT-Based Electrochemical Sensors and Biofuel Cells: Combining Intrinsic and Design-Induced Stretchability," *Nano Lett.*, vol. 16, no. 1, pp. 721–727, 2016.
- [115] W. Jia, G. Valdés-Ramírez, A. J. Bandodkar, J. R. Windmiller, and J. Wang, "Epidermal Biofuel Cells: Energy Harvesting from Human Perspiration.," *Angew. Chem. Int. Ed. Engl.*, vol. 52, no. 28, pp. 7233–7236, Jul. 2013.
- [116] Y. Ogawa, Y. Takai, Y. Kato, H. Kai, T. Miyake, and M. Nishizawa, "Stretchable biofuel cell with enzyme-modified conductive textiles," *Biosens. Bioelectron.*, vol. 74, pp. 947–952, 2015.
- [117] S. J. Konopka and B. McDuffie, "Diffusion coefficients of ferri- and ferrocyanide ions in aqueous media, using twin-electrode thin-layer electrochemistry," *Anal. Chem.*, vol. 42, no. 14, pp. 1741–1746, 1970.
- [118] M. Smolander, H. Boer, M. Valkiainen, R. Roozeman, M. Bergelin, J.-E. Eriksson, X.-C. Zhang, A. Koivula, and L. Viikari, "Development of a printable laccase-based biocathode for fuel cell applications," *Enzyme Microb. Technol.*, vol. 43, no. 2, pp. 93–102, Aug. 2008.
- [119] C. Lau, E. R. Adkins, R. P. Ramasamy, H. R. Luckarift, G. R. Johnson, and P. Atanassov, "Design of Carbon Nanotube-Based Gas-Diffusion Cathode for O₂ Reduction by Multicopper Oxidases," *Adv. Energy Mater.*, vol. 2, no. 1, pp. 162–168, Jan. 2012.
- [120] G. P. M. K. Ciniciato, C. Lau, A. Cochrane, S. S. Sibbett, E. R. Gonzalez, and P. Atanassov, "Development of paper based electrodes: From air-breathing to paintable enzymatic cathodes," *Electrochim. Acta*, vol. 82, pp. 208–213, Nov. 2012.

- [121] S. Tuurala, M. Smolander, J. Uotila, O.-V. Kaukonieni, H. Boer, M. Valkiainen, A. Vaari, A. Koivula, and P. Jenkins, "Performance of a Printable Enzymatic Fuel Cell: Study on Mediated ThL Laccase Cathode," *ECS Trans.*, vol. 25, no. 33, pp. 1–10, 2010.
- [122] J. Keskinen, E. Sivonen, M. Bergelin, J. E. Eriksson, P. Sjöberg-Eerola, M. Valkiainen, M. Smolander, A. Vaari, J. Uotila, H. Boer, and S. Tuurala, "Printed Supercapacitor as Hybrid Device with an Enzymatic Power Source," *Adv. Sci. Technol.*, vol. 72, pp. 331–336, Oct. 2010.

Appendix A: Electron transfer properties of ferro/ferricyanide on DuPont ink

Electron transfer properties of DuPont ink were studied on a glassy carbon (GC, $r = 2.5$ mm) electrode. Figure A1 shows the CV measurements (a-c) at different scan rates, and Randles-Ševčík plots (d) of three different electrodes: 1) GC, 2) GC coated with $4 \mu\text{l}$ of DuPont ink, and 3) GC coated with $4 \mu\text{l}$ of DuPont ink modified with MWCNTs (as in Publications II and III).

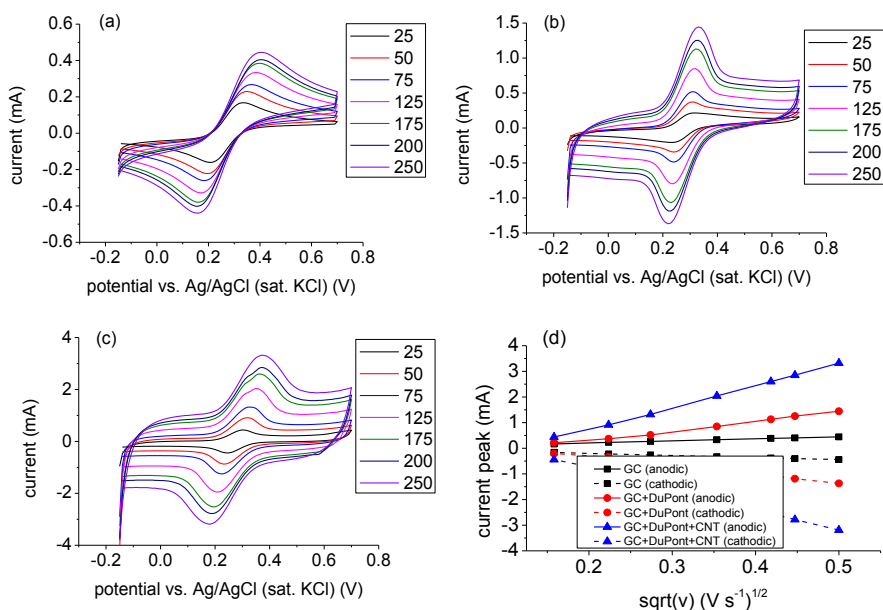


Figure A1. Cyclic voltammograms of (a) GC, (b) GC coated with DuPont ink, (c) GC coated with MWCNT-modified DuPont ink using different scan rates (mV s^{-1}), and (d) Randles-Ševčík plots of the electrodes studied. The electrolyte contained $7.5 \text{ mM F}_3\text{Fe}(\text{CN})_6/\text{F}_4\text{Fe}(\text{CN})_6$ in 1 M KCl . The counter electrode was Pt-wire and the reference electrode Ag/AgCl (sat. KCl). (Unpublished)

The slopes in the Panel (d) vary with the modification of the electrodes, which implies varying electrode surface area. The diffusion coefficient of the reactant can be calculated from the slopes. The slope of the GC electrode is 7.8×10^{-4} and Equation (18) leads to $D = 4 \times 10^{-6} \text{ cm}^2 \text{ s}^{-1}$, which is rather close to the literature values (ca. $7 \times 10^{-6} \text{ cm}^2 \text{ s}^{-1}$ [117]). For coated electrodes, the diffusion coefficient is assumed to be the same and the change in the slopes is attributed to an increased active area. The slope for GC/DuPont is 4.1×10^{-3} and for GC/MWCNT-modified DuPont 8.4×10^{-3} ; hence doping with MWCNTs increased the active area of the electrode twofold. This was also observed by Smolander et al. [118], their measurements showed twofold higher current densities for MWCNT-modified DuPont ink containing ThL and ABTS.

Appendix B: Studying DET of ThL and rMaL in a fuel cell setup

One approach to increase the cell voltage is to utilise DET at the cathode, and hence DET of both ThL and rMaL was studied. Both laccases were immobilised on Toray paper (TGP-H-060, Fuel Cells Etc) and teflonised CB (prepared as in [119]). The electrolyte used in the measurements was 100 mM potassium phosphate buffer (KPB) with varying pH.

Toray paper electrodes

ThL solution was prepared by pipetting 100 μl of ThL (activity 156 U ml^{-1}) into 1.85 ml of KPB (pH 5), resulting in an enzyme activity of 8 U ml^{-1} . rMaL solution was prepared by pipetting 100 μl of rMaL (rMaL 138 U ml^{-1}) into 1.625 ml of KPB (pH 5), resulting in an enzyme activity of 8 U ml^{-1} . A piece of Toray paper was washed with ethanol and distilled water and dried at room temperature. Eight pieces were cut using a punching tool ($r = 2.5 \text{ mm}$) and soaked into laccase solutions (four each) overnight at 4 $^{\circ}\text{C}$.

The samples were measured the next day, attaching the Toray paper electrode on a glassy carbon electrode with a cup-formed holder made of Teflon. The measurement was made by measuring OCV for 1 h and then performing a CV from 800 mV to 0 mV vs. Ag/AgCl at a scan rate of 10 mV s^{-1} . The CV scan was repeated three times with 3 different samples.

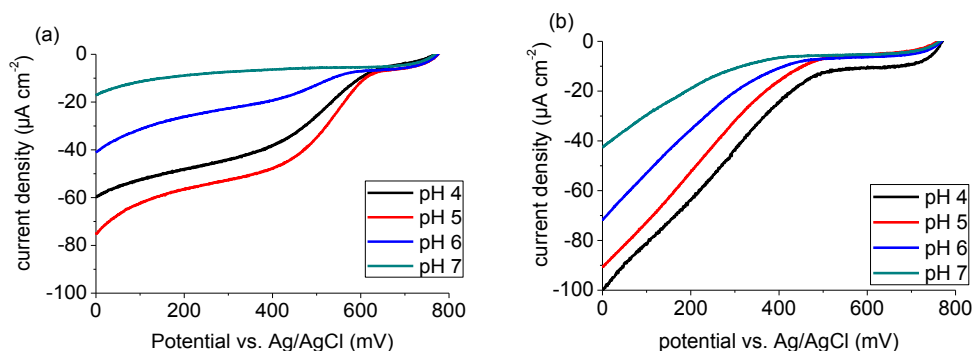


Figure B1. Cyclic voltammograms at varying pH of (a) ThL and (b) rMaL immobilised into Toray paper. Scan rate 10 mV s^{-1} . The electrolyte was bubbled with O_2 . The curves represent average values of the third scan ($n = 3$). (Unpublished)

Cyclic voltammograms of the Toray paper electrodes in different pH values are shown in Figure B1. Both laccases indicated ORR without any use of a mediator, meaning that they were successfully immobilised into the Toray paper. The ORR starts at rather high potential with ThL, at ca. 600 mV vs. Ag/AgCl, which makes it a good cathode enzyme for BFC or battery applications. However, ThL is very sensitive to pH, showing its highest catalytic current at pH 5 but almost deactivating at pH 7. ThL also shows an interesting CV curve. The catalytic current of ORR increases dramatically between 600 and 500 mV vs. Ag/AgCl, but plateaus after that. rMaL on the other hand starts to catalyse ORR at ca. 500 mV vs. Ag/AgCl, with increasing catalytic current throughout the potential window. In addition, rMaL is not as sensitive to pH as ThL, still

catalysing ORR at pH 7. For this reason, rMaL could be a better cathode enzyme than ThL to couple with pH-sensitive anode enzymes.

Teflonised CB electrodes

ThL solution was prepared by pipetting 10 μl of ThL (780 U ml^{-1}) into 4.99 ml of KPB (pH 5), resulting in an enzyme activity of 1.56 U ml^{-1} . rMaL solution was prepared by pipetting 50 μl of rMaL (138 U ml^{-1}) into 4.95 ml of KPB (pH 5), resulting in an enzyme activity of 1.38 U ml^{-1} .

Toray paper was cut into a piece as illustrated in Figure B2. Small holes were punched in order to increase air diffusion through the material. 100 mg of teflonised CB was pressed onto Toray paper forming a round ($r = 1.5 \text{ cm}$) area (see [120] for more details). 10 μl of ethanol was dropped on the teflonised CB and soaked into laccase buffer solution overnight at 4 $^{\circ}\text{C}$. Three similar samples were prepared using both laccases.

The samples were measured the next day. The measurement setup is illustrated in Figure B2. A rectangular piece of filter paper (Whatman[®]) was placed between the laccase electrode and a Pt mesh. The cell was clamped together with a paperclip. The other end of the filter paper was soaked into KPB (pH 5), which caused the electrolyte to rise up into the cell. Ag/AgCl reference electrode was inserted into the electrolyte. OCV was measured for 1 h and CA was performed after that in 50 mV steps every 10 min from OCV to 0 V.

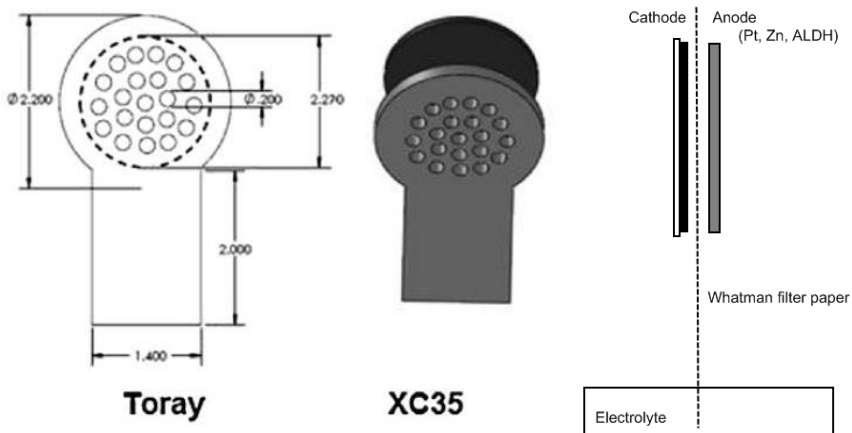


Figure B2. Left: schematic of the teflonised CB electrode (reprinted from [120] with permission). Right: Schematic of the test electrode setup. (Unpublished)

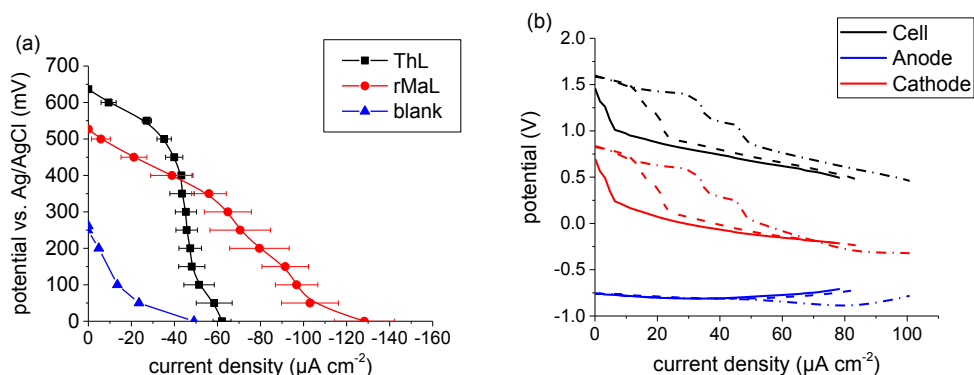


Figure B3. (a) Curves of CA measurement of teflonised CB laccase electrodes. Geometrical electrode area 7 cm^2 . (b) Individual electrode potentials of CP measurement of $\text{Zn}^{\text{n sol.}}||\text{ThL}/\text{ABTS}$ cells. The printed cathodes contained different amounts of active components: 1x (solid), 10x (dash), and 100x (dash-dot). Geometrical cell area 6.25 cm^2 . The original data was presented by Tuurala et al. in Figure 5 in [121]. Here the curves represent the average data ($n = 2$). (Unpublished)

CA measurements in Figure B3a showed that both laccases immobilised in teflonised CB catalyse ORR via DET. ThL electrodes have ca. 100 mV higher potential than rMaL electrodes between current densities $0\text{--}50 \mu\text{A cm}^{-2}$, but after that the potential of ThL electrodes drops dramatically. rMaL electrodes on the other hand maintain their potential, which decreases almost linearly between current densities $50\text{--}100 \mu\text{A cm}^{-2}$.

This behaviour of ThL at higher current densities was also observed in the author's earlier transaction publication [121]. Curves of individual electrode potentials from CP measurement of printed ThL/ABTS electrodes paired with solid Zn anode are shown in Figure B3b. Different amounts of ThL/ABTS were used in the inks. It was shown that increased amounts of catalytic components maintain the cathode, and thus cell potential, higher as current density increases. The highest OCV was 1.6 V, which corresponds to a cathode potential of 0.84 V.

This data indicated that ThL can catalyse ORR at high potential (ca. 700–800 mV), as long as the pH is between 4 and 5 and there is sufficient enzyme to keep the catalytic current high. rMaL on the other hand catalyses ORR at lower potential than ThL but tolerates neutral pH better. For this reason, it is important to know the application requirements for the cathode before the enzyme is selected.

Appendix C: A stack of biobatteries combined with printed supercapacitors

The use of biobatteries in mW-scale applications is still a question due to their modest power output. Therefore, the combination of printed biobatteries and printed supercapacitors was tested. In order to obtain higher voltage, three 12.25 cm² ALDH/ThL biobatteries with TMPD and ABTS mediators, prepared as in Publications II and III, were connected in series, creating an OCV of ca. 1.7 V. This stack was connected with two series-connected printed carbon-based supercapacitors (prepared as in [122]). The capacitance of the supercapacitors stack was approximately 0.2 F and the leakage current was 3 μ A at 1.2 V.

Both the stack of biobatteries and the stack of supercapacitors (pre-charged to 1 V) were subjected to a pulse test in which 5 mA pulses were drawn for 3 s while the potential was measured. The time between each pulse was 20 min. It was seen that three cells alone could not maintain the voltage (inset in Figure C1), and that the supercapacitors worked well, although the potential decreased during the pulses (Figure C1). In order to maintain the potential, a power source is needed to charge the supercapacitors between the pulses. Hence, the stack of supercapacitors was charged again to 1 V and connected with the stack of biobatteries. The same type of pulsing test was repeated, except that the first four pulses were taken every 10 min, after which they were taken every 20 min. The potential of the system remained at ca. 1 V for 10 hours, after which it started to decrease dramatically.

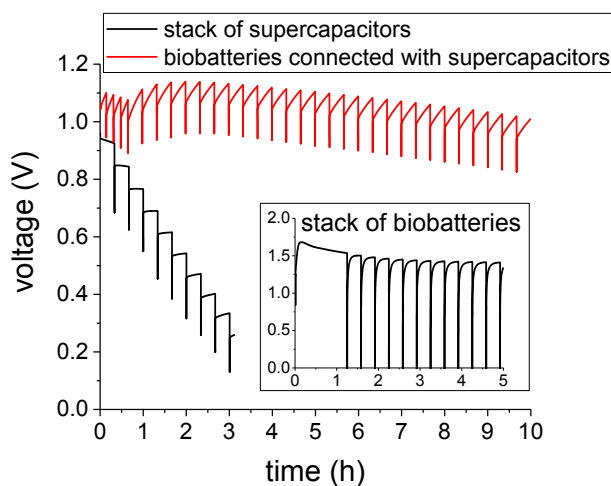


Figure C1. Voltage vs. time plot as a stack of biobatteries (inset), supercapacitors and a hybrid combination of both are discharged with pulses of 5 mA for 3 s. (Unpublished)

This measurement showed that printed biobatteries can be connected successfully with printed supercapacitors. The charging time of the capacitor between current pulses must be taken into account due to its high impact on the system performance. When these two stacks were connected, their combination was able to provide energy peaks of 12-17 mWs every 20 min for 15 h.

Printed enzymatic glucose/air batteries

The enzymatic biofuel cell (EBFC) converts the chemical energy of biofuel into electricity via bioelectrochemical reactions. In this thesis, laminar EBFCs were assembled using printed enzymatic electrodes and characterised by means of electrochemistry.

The performance of the printed EBFCs was in the range of microwatts. The power output could be increased by adding biocatalysts and active electrode area. **The stability** of printed and hot-dried enzymatic electrodes was 60-80% after 28 days of storage at room temperature. Incorporating mediators into the inks degraded the electrodes faster and only 20-30% of the enzymatic activity was maintained during the same storage time.

The mass-manufacturing of printed EBFCs was demonstrated on VTT's modular roll-to-roll screen printer. The performance of the EBFCs manufactured at the pilot facility was 10-50% of the laboratory manufactured EBFCs, due to decreased amount of active components in the inks and elevated drying temperatures of the inks.



ISBN 978-952-60-7412-2 (printed)

ISBN 978-952-60-7411-5 (pdf)

ISSN-L 1799-4934

ISSN 1799-4934 (printed)

ISSN 1799-4942 (pdf)

978-951-38-8537-3 (printed)

978-951-38-8536-6 (pdf)

2242-119X

2242-119X (printed)

2242-1203 (pdf)

Aalto University
School of Chemical Engineering
Department of Chemistry and Materials Science
www.aalto.fi

BUSINESS +
ECONOMY

ART +
DESIGN +
ARCHITECTURE

SCIENCE +
TECHNOLOGY

CROSSOVER

DOCTORAL
DISSERTATIONS